

AD-A135 590

CENTRIFUGAL AND NUMERICAL MODELING OF BURIED STRUCTURES  
VOLUME 1 EXECUTIVE SUMMARY COLORADO UNIV AT BOULDER DEPT OF  
CIVIL ENVIRONMENTAL AND ARCH H RO 14 JUL 84  
AFOSR-TP-87-1352 AFOSR-84-0300

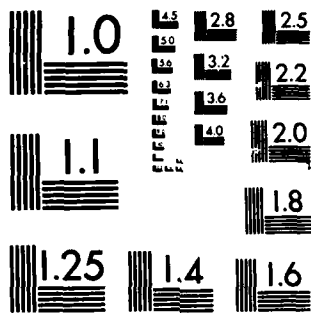
1/1

UNCLASSIFIED

F 19/9

NL

END  
DATE  
FILMED  
1-81



MICROCOPY RESOLUTION TEST CHART  
NATIONAL BUREAU OF STANDARDS-1963-A

2

REPORT DOCUMENTATION PAGE			
AD-A185 590-DTIC		DTIC FILE COPY	
1a. SECURITY CLASSIFICATION AUTHORITY <b>SELECTED</b>		1b. RESTRICTIVE MARKINGS	
2b. DECLASSIFICATION/DOWNGRADING SCHEDULE <b>OCT 01 1987</b>		3. DISTRIBUTION/AVAILABILITY OF REPORT Approved for public release; distribution is unlimited	
4. PERFORMING ORGANIZATION REPORT NUMBER(S) <b>CAD</b>		5. MONITORING ORGANIZATION REPORT NUMBER(S) <b>AFOSR-TR-87-1352</b>	
6a. NAME OF PERFORMING ORGANIZATION University of Colorado	6b. OFFICE SYMBOL (If applicable) CEAE Dept.	7a. NAME OF MONITORING ORGANIZATION AFOSR/NA	
6c. ADDRESS (City, State, and ZIP Code) Civil, Environmental & Architectural Engr. Campus Box 428, Boulder, CO 80309-0428		7b. ADDRESS (City, State, and ZIP Code) Bldg. 410 Bolling AFB, DC 20332-6448	
8a. NAME OF FUNDING/SPONSORING ORGANIZATION Air Force Office of Scientific Research	8b. OFFICE SYMBOL (If applicable) AFOSR/NA	9. PROCUREMENT INSTRUMENT IDENTIFICATION NUMBER AFOSR-84-0300	
8c. ADDRESS (City, State, and ZIP Code) Bldg. 410 Bolling AFB, DC 20332-6448		10. SOURCE OF FUNDING NUMBERS	
		PROGRAM ELEMENT NO. 61102F	PROJECT NO. 2302
		TASK NO. C1	WORK UNIT ACCESSION NO.
11. TITLE (Include Security Classification) (U) Centrifugal and Numerical Modeling of Buried Structures; Vol. 1: Executive Summary			
12. PERSONAL AUTHOR(S) Ko, Hon-Yim			
13a. TYPE OF REPORT Final	13b. TIME COVERED FROM TO	14. DATE OF REPORT (Year, Month, Day) 7/14/87	15. PAGE COUNT 49
16. SUPPLEMENTARY NOTATION			
17. COSATI CODES		18. SUBJECT TERMS (Continue on reverse if necessary and identify by block number)	
FIELD	GROUP	SUB-GROUP	
19. ABSTRACT (Continue on reverse if necessary and identify by block number) This volume is an executive summary of the research project on centrifugal and numerical modeling of buried structures subjected to static and dynamic loadings on the ground surface. Techniques were developed for testing model buried pipes in a geotechnical centrifuge. An impact generator was developed for applying an airblast loading on the centrifuge model. A dynamic stress gage was developed for measuring the stresses generated in the soil and acting on the buried pipe during the airblast loading. Finite element analyses were performed on the buried pipe experiments. Comparison between centrifuge test data and analytical results is used to validate the numerical analysis procedure. <i>Keywords:</i>			
20. DISTRIBUTION/AVAILABILITY OF ABSTRACT <input checked="" type="checkbox"/> UNCLASSIFIED/UNLIMITED <input type="checkbox"/> SAME AS RPT <input type="checkbox"/> DTIC USERS		21. ABSTRACT SECURITY CLASSIFICATION Unclassified	
22a. NAME OF RESPONSIBLE INDIVIDUAL Dr. Spencer T. Wu		22b. TELEPHONE (Include Area Code) (202) 767-6962	22c. OFFICE SYMBOL NA

**CENTRIFUGAL AND NUMERICAL  
MODELING OF BURIED STRUCTURES**

**Vol. 1**

**EXECUTIVE SUMMARY**

**by**

**Hon-Yim Ko**

CENTRIFUGAL AND NUMERICAL  
MODELING OF BURIED STRUCTURES

Vol. 1

EXECUTIVE SUMMARY

by

Hon-Yim Ko

FINAL REPORT TO THE AIR FORCE OFFICE OF SCIENTIFIC RESEARCH

ON GRANT NO. AFOSR-84-0300

"CENTRIFUGAL AND NUMERICAL MODELING OF BURIED STRUCTURES"

FOR PERIOD SEPTEMBER 1, 1984 TO FEBRUARY 28, 1987

by

Hon-Yim Ko

University of Colorado, Boulder, Colorado 80309

VOLUME 1: EXECUTIVE SUMMARY

1. INTRODUCTION

This research grant was initiated in September, 1984 for research to develop techniques for modeling the performance of buried structures under surface loadings that are either static or dynamic. Modeling by numerical techniques as well as by physical testing in the increased gravity environment in a centrifuge was to be attempted. In addition to the development of the centrifuge testing procedure and of finite element analysis techniques to incorporate the soil-structure interaction phenomena, a primary goal for the research was to seek verification of the numerical modeling technique through comparison with the centrifuge test results. The rationale behind such verification procedure is that in the centrifuge tests the soil properties and boundary conditions are well controlled, while at the same time the gravity loading in the centrifuge makes it possible to simulate the self-weight induced stresses that govern the soil-structure interaction phenomena.

The first part of the research dealing with static loading of buried structures is a continuation of a previous grant from AFOSR, Grant No. 81-0072. Results from this part of the project will be summarized in Volume 1, Executive Summary, of this report. Results of the second part of the research in which dynamic loadings of buried structures were the focus of the investigation are presented in Volumes 2 and 3, and are also summarized in Volume 1.

2. MODELING OF BURIED PIPES UNDER STATIC LOADING

The configuration of the buried structure chosen for the study is a circular pipe, which can be considered to represent a class of underground structures that includes

↓	
<input type="checkbox"/>	
<input type="checkbox"/>	
Codes	
Dist	Avail and/or Special
A-1	



shelters for horizontally buried missiles and oil or gas pipelines. Structures with more complex geometries (e.g., box structures) are easily substituted and present no particular difficulties in modeling except for additional efforts in building the model for both the numerical analysis and the physical testing. The simplest, yet realistic geometry of a circular pipe was chosen without loss of generality. A flexible pipe buried at a shallow depth was chosen for the centrifuge tests, so as to accentuate the soil-structure interaction aspects.

Centrifuge experiments were conducted in the 10 g-ton centrifuge at the University of Colorado and were carried out at 50 g on a 4-in. diameter, 15.9 in. long aluminum pipe with a wall thickness of 0.025 in. The scale factor for length in centrifuge modeling is inversely proportional to the gravity ratio, so that the prototype being modeled with these tests is a pipe with dimensions 50 times greater than the model size. The pipe was buried with the crown at a depth equal to the pipe diameter. Strain gages were mounted on both the inside and the outside of the pipe around the circumference in order to measure the deformations of the pipe and, from these deformations, to calculate the stresses that caused them. A rigid rod was independently mounted inside the pipe on the walls of the model container so as to be unaffected by the soil and pipe deformations. From this rod, LVDT's were mounted to measure the radial deflection of the pipe at 11 locations around the pipe. The strain gages and the LVDT's were all located in one longitudinal section of the pipe so that the results could be correlated to portrait the pipe performance at one location along its length.

The loads were applied by a pressure bag mounted over the soil surface either symmetrically or asymmetrically over a 4-in. wide area over the entire length of the pipe. Regulated air pressure was applied through this bag in increments of 10 psi.

The soil used in this study was a sandy silt and the model for centrifuge testing was prepared by a static undercompaction method designed to achieve uniform density. The model was prepared in two halves that were separated at the horizontal plane passing through the springline of the pipe. Semi-cylindrical troughs were precisely trimmed from these halves so that the model pipe could be located in a snug fit in this trough. A narrow groove was cut in the soil trough at the section where the strain gages were located on the pipe to avoid direct contact between the soil and the strain gages which might otherwise damage the gages. However, subsequent analysis of the strain gage data showed that this was a poor decision, since the lack of uniform contact produced localized stresses at the gage locations

which invalidated the strain gage readings. Therefore, the pipe deflections measured by the LVDT's constituted the primary experimental data from the centrifuge tests.

Analytical modeling of the buried pipe under static loading applied on the soil surface was carried out using the finite element method. A key ingredient is the selection of the constitutive relations for the soil, whereas the algorithm chosen for the numerical integration also plays an important role in the accuracy of the numerical results. In this part of the study, 4-node quadrilateral elements were used to model the soil-pipe system. Under-integration was used for elements modeling the flexible pipe to ensure that shear locking does not make the pipe elements appear unduly stiff.

Three types of constitutive relations were used in modeling the soil: linear elastic, hyperbolic (nonlinear) and elasto-plastic (specifically, Lade's relation). The silty soil used in the centrifuge experiments were tested to obtain a suite of laboratory data for the purpose of calibrating these constitutive models.

In the numerical analysis, the boundary and loading conditions used in the centrifuge tests were precisely simulated, including the loading history experienced by the soil during spin-up of the centrifuge. In this way, exact correspondence between experiment and analysis is established. The data on the buried pipe performance from the experiments, obtained under simulated full scale prototype conditions, provides the basis for validating the accuracy of the numerical method.

Both symmetrical and asymmetrical loadings were simulated. The calculated deflections of the pipe are shown in Fig. 1 to 8, where comparison with the experimental data is made. In Figs. 1 to 4, the deflections under symmetrical loading of 10, 20, 30 and 40 psi are compared with the calculated values using both the hyperbolic and Lade's constitutive models. It is seen that the correct shape was predicted for the deformed pipe. Both analyses underestimated the pipe deflections at the crown and the springline, whereas the deflections near the invert are fairly well predicted. In Figs. 5 to 8, the deflections under asymmetrical loads are compared. Again, the calculated values are smaller than the experimental results.

An explanation for the discrepancy can be found by examining the stress paths experienced by various soil elements surrounding the pipe. In Fig. 9, three elements A, B and C are identified. The calculated stress paths for them using Lade's model are shown in Fig. 10. The stress path for element C, which is located at the invert of the

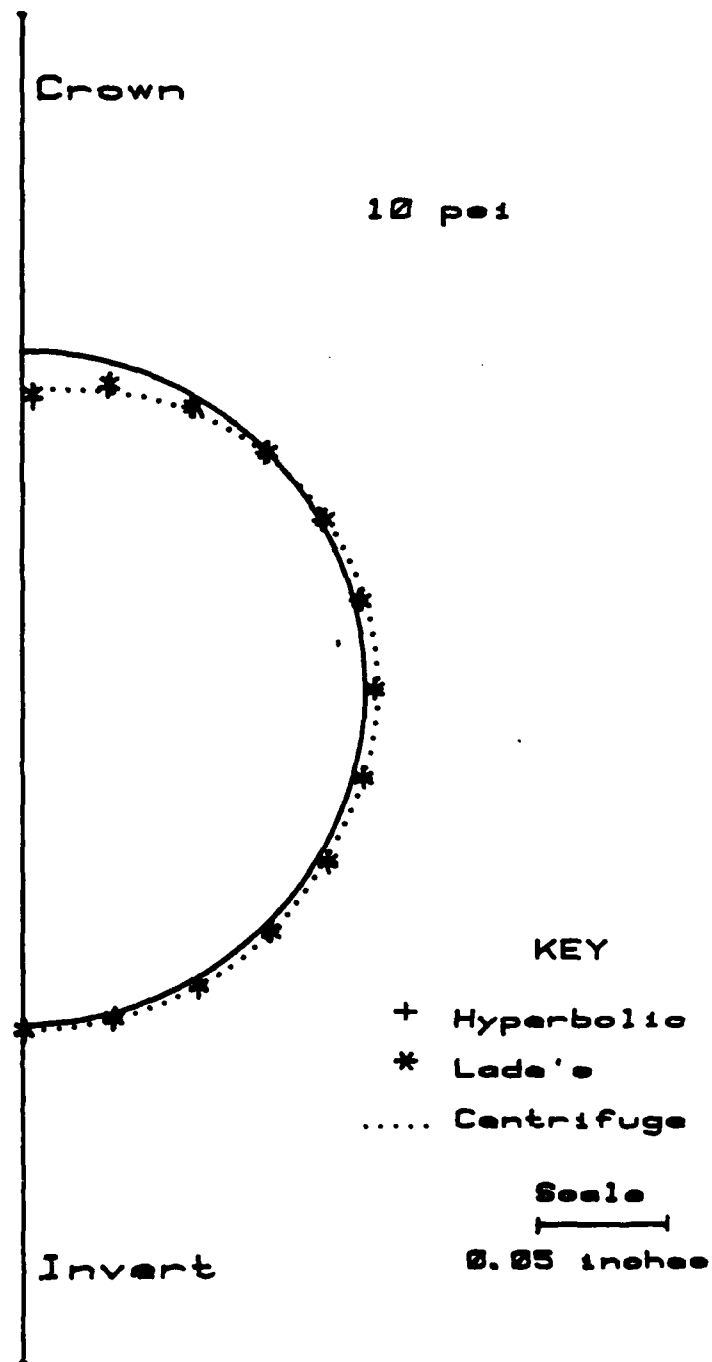


Figure 1. Comparison of Deflections.  
Symmetrical Load 10 psi

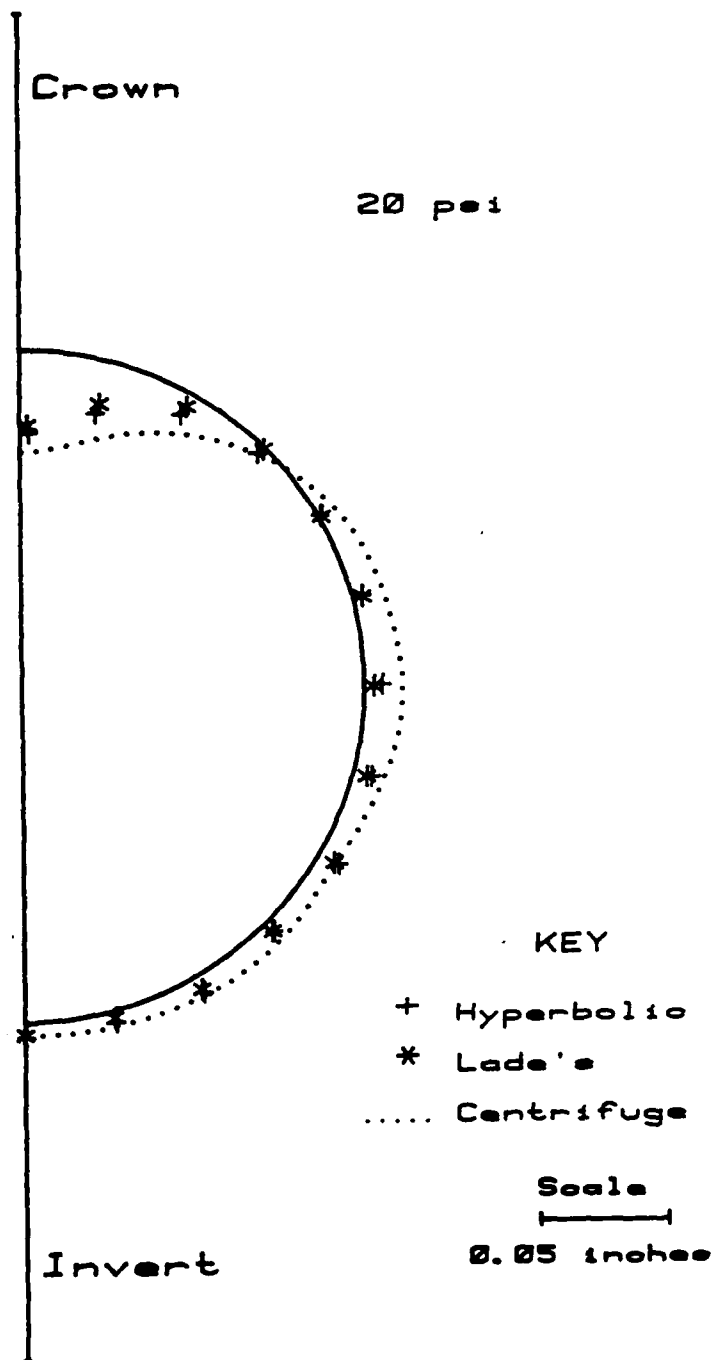


Figure 2. Comparison of Deflections.  
Symmetrical Load 20 psi

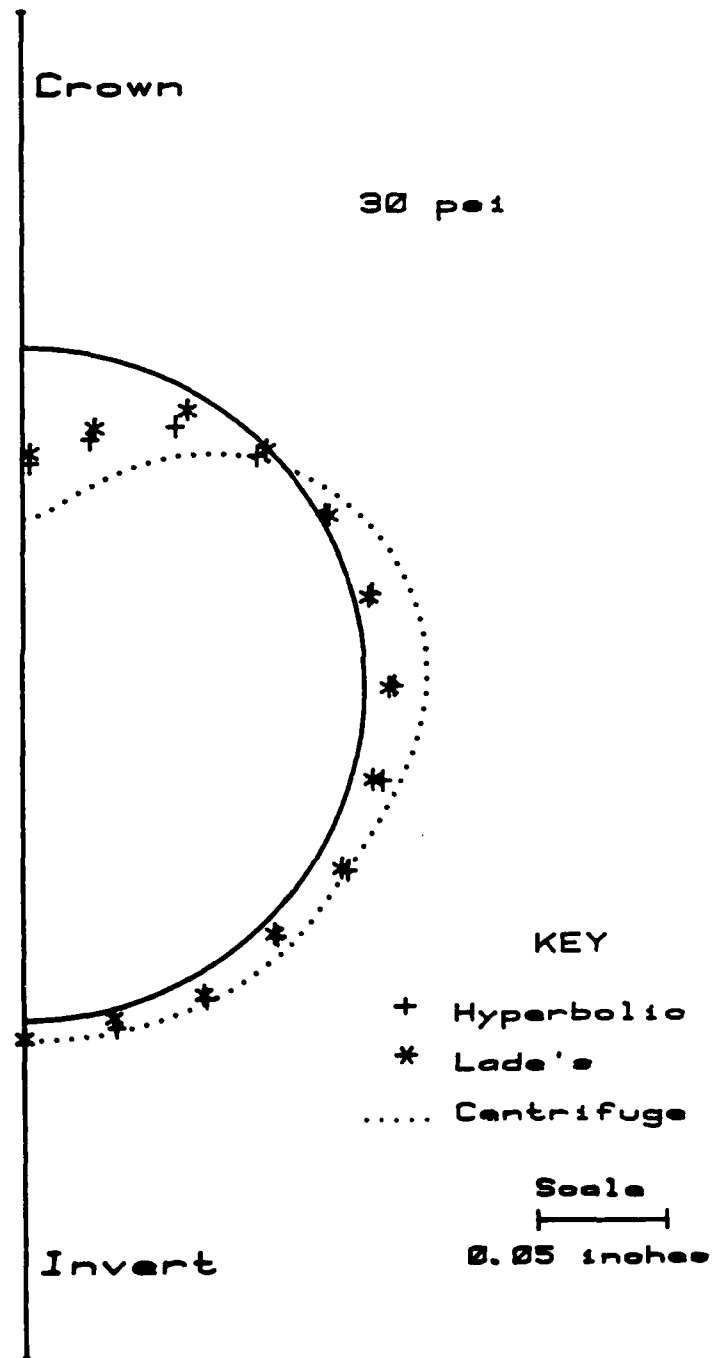


Figure 3. Comparison of Deflections.  
Symmetrical Load 30 psi

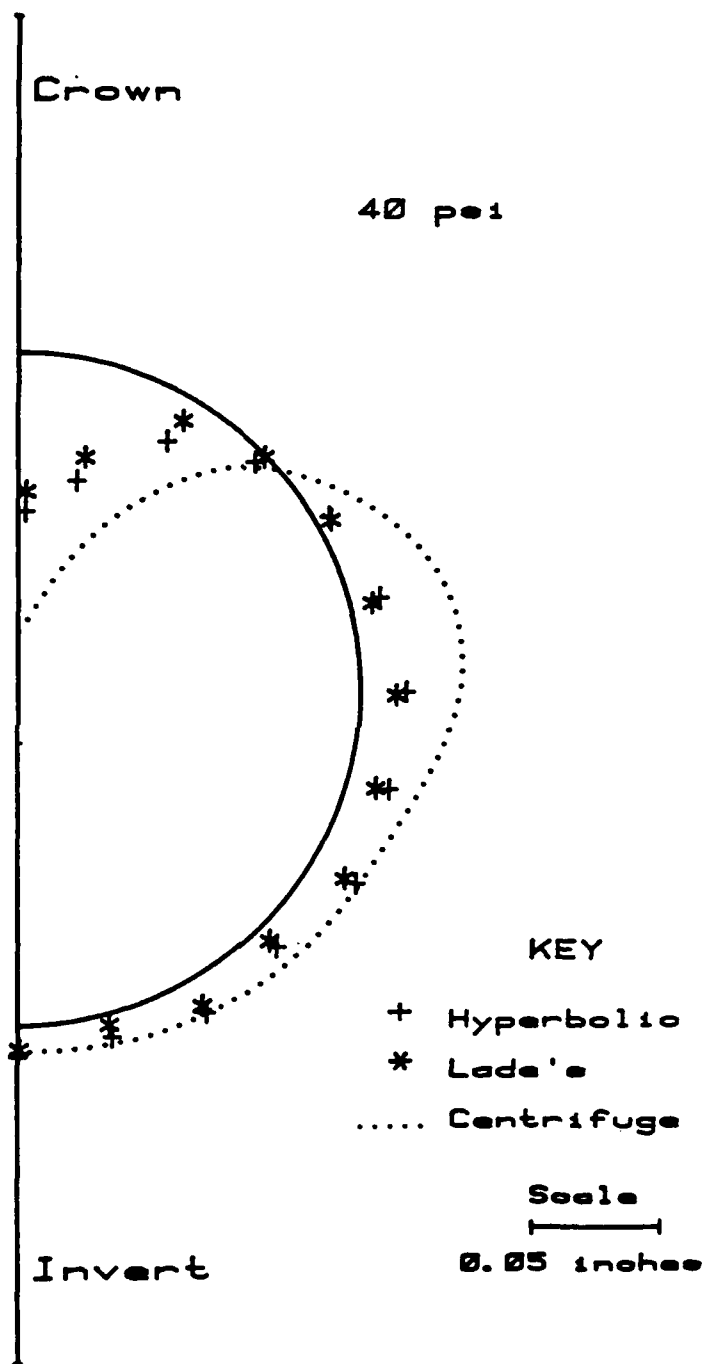


Figure 4. Comparison of Deflections.  
Symmetrical Load 40 psi

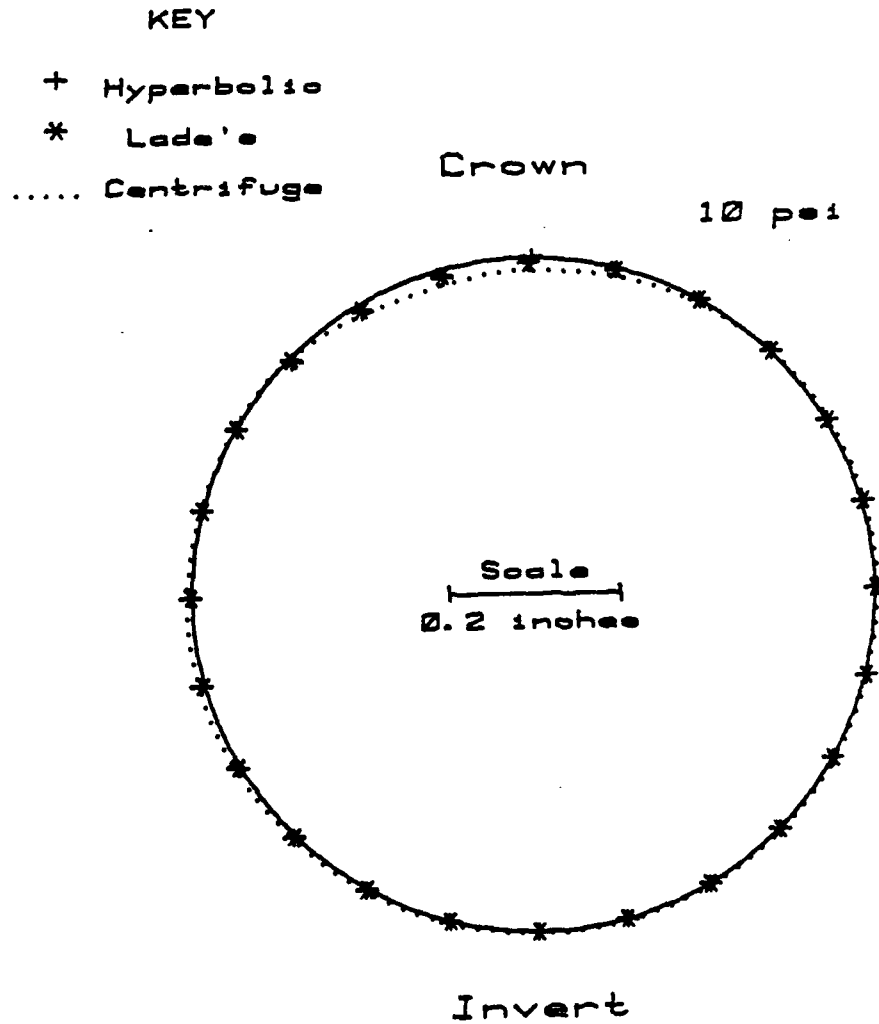


Figure 5. Comparison of Deflections.  
 Unsymmetrical Load 10 psi

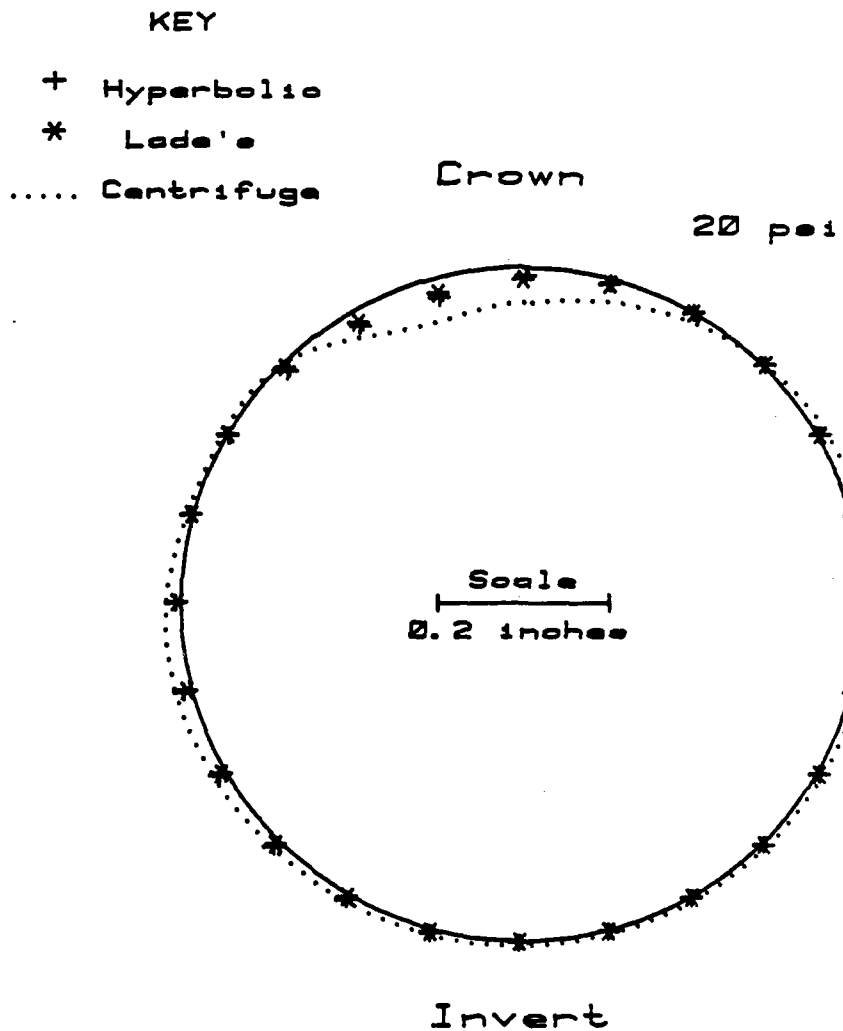


Figure 6. Comparison of Deflections.  
Unsymmetrical Load 20 psi

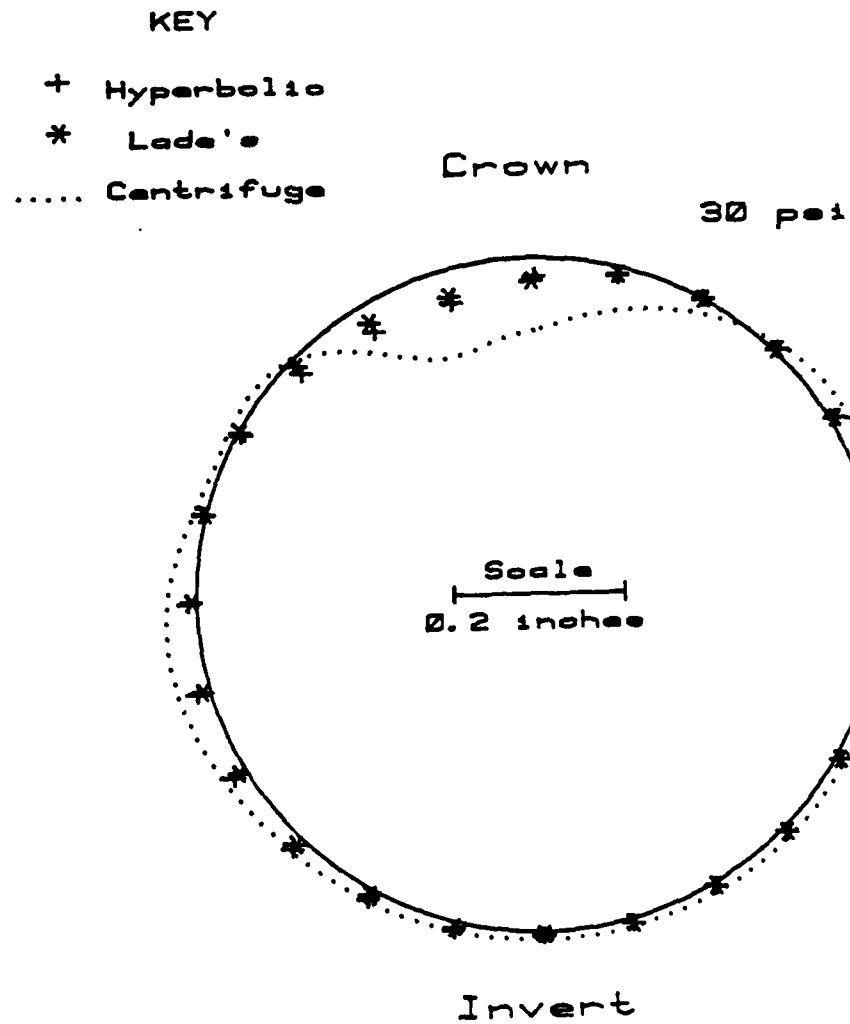


Figure 7. Comparison of Deflections.  
 Unsymmetrical Load 30 psi

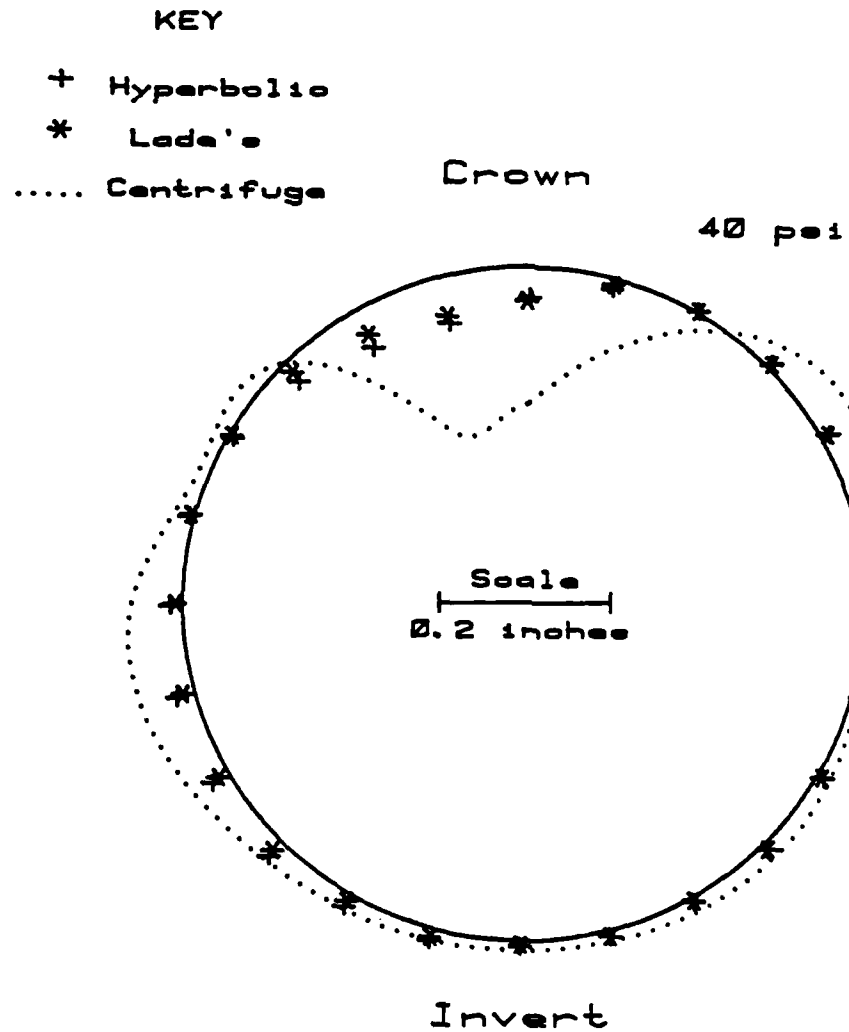


Figure 8. Comparison of Deflections.  
Unsymmetrical Load 40 psi

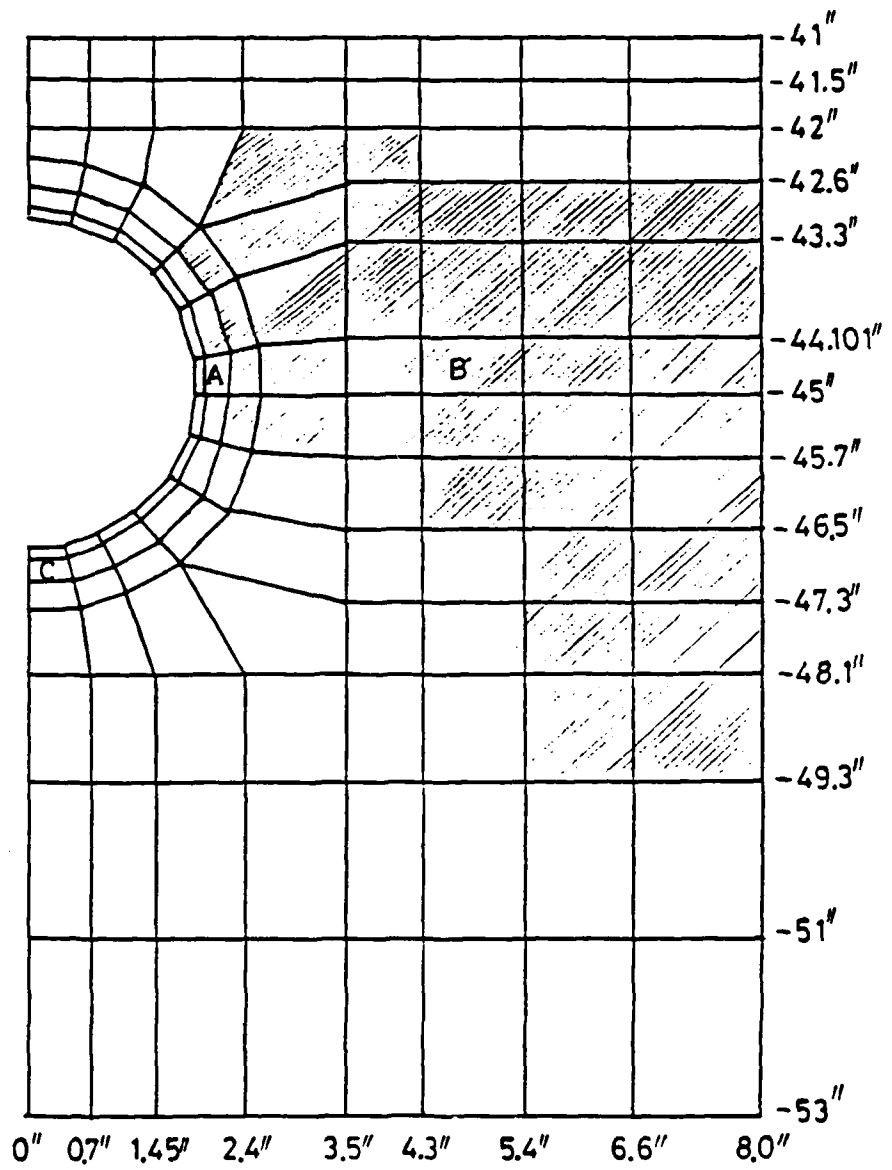


Figure 9. Stiffer Elements in Mesh 3

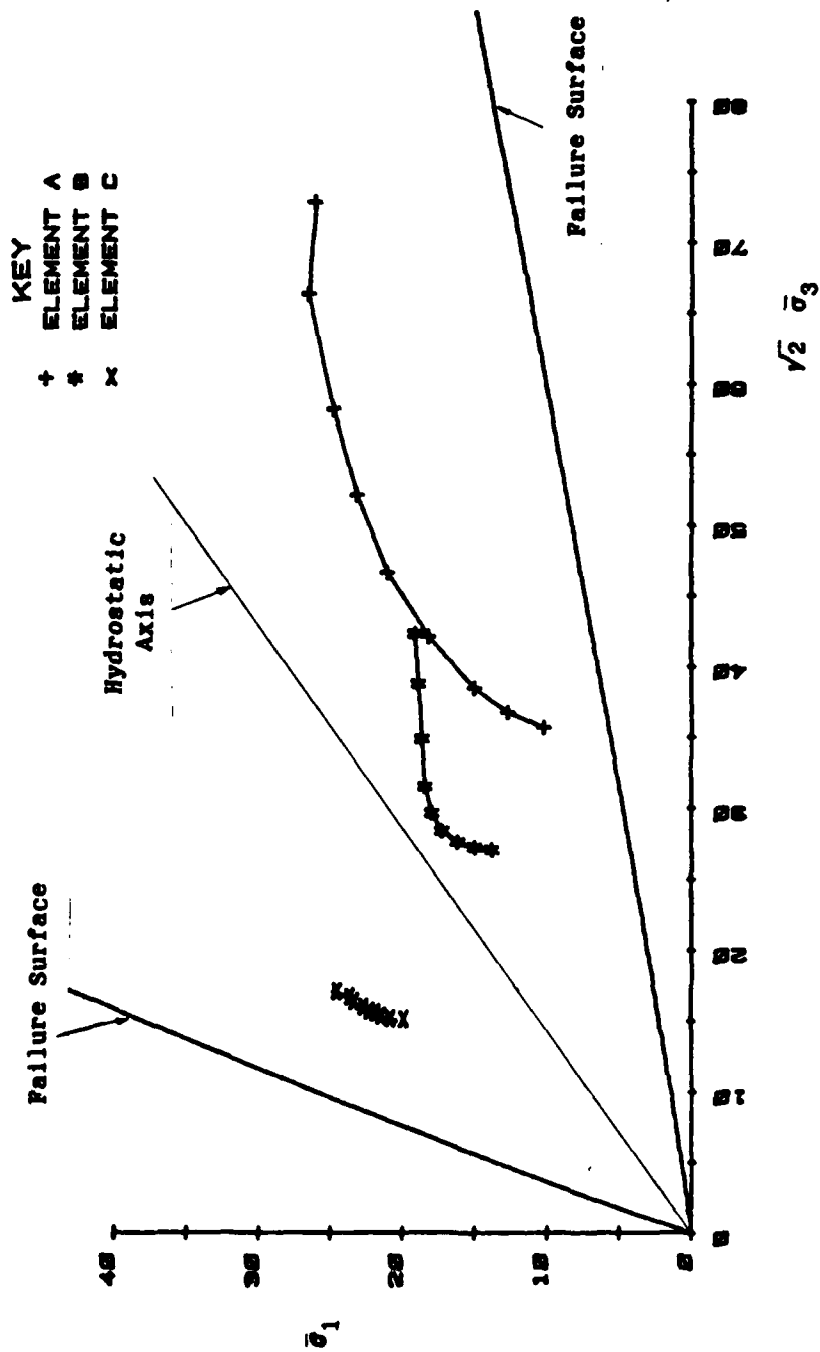


Figure 10. Stress Paths. Lade's Soil Model

pipe, shows that under symmetrical surface loading the stress changes at C are very similar to those experienced by a soil sample tested under conventional triaxial compression (CTC) condition, which is the condition used for obtaining the soil properties for calibrating the constitutive models. It is, therefore, reasonable that the deflections measured near the invert would be well predicted by the numerical results. On the other hand, the stress path for element A, which is located at the pipe springline, shows that the soil first experienced unloading in terms of the shear stress (as measured by the perpendicular distance from the hydrostatic axis) before reloading in shear, while the mean stress (as measured by the distance parallel to the hydrostatic axis) was increasing all the time. In the numerical analysis, a criterion had to be adopted for defining loading, unloading and reloading, which is based on the magnitude of the shear stress. Thus, the region of soil around element A was experiencing unloading and reloading, and hence a soil modulus appropriate for unloading and reloading was used to calculate the response of the region of soil which is shown shaded in Fig. 9. This region includes element B whose stress path is also shown in Fig. 10. Because the modulus for unloading and reloading is invariably higher than that for loading in any constitutive model, it produced a stiffer response of the soil in the region containing A and B, and consequently a smaller deflection of the pipe at the springline and, subsequently, at the crown.

A second consideration which arises from examining the stress paths in Fig. 10 is that as elements A and B continue their loading, their stress path directions are now more aligned with that which is followed by conventional triaxial extension (CTE) testing. If the soil had been isotropic and remained as such during the process, constitutive models calibrated on CTC test results would perform satisfactorily. However, soils develop stress induced anisotropy during loading. In addition, the soil used in the centrifuge experiments was compacted in layers and certainly contained a significant degree of anisotropy. It is, therefore, concluded that the use of isotropic constitutive models to represent the soil properties was not appropriate and had led to less than adequate analytical results. However, the state of the art in constitutive modeling of soils is such that no viable anisotropic plasticity model exists which can be easily implemented in numerical analysis for the study of soil structure interaction phenomena.

### 3. MODELING OF BURIED PIPES UNDER DYNAMIC LOADING

The research on the behavior of buried pipes under dynamic loading included several components. The first involved the development of a method of generating an impulse load. The second dealt with the development of a

stress gage for measuring the dynamic stresses generated in the soil and at the interface between the pipe and the soil. The third component was concerned with the production of a micro-concrete that could be used in constructing the model pipes in the centrifuge tests. The fourth component was a centrifuge test program in which a parametric study was made of the factors that were considered to have primary influence on the response of a buried pipe. Finally, the implementation of a finite element program for studying the dynamic loading effect on the buried pipe was needed to analyze the centrifuge experiments. These aspects of the research are described in the following sections.

#### A. Impact Generator

After considering several alternatives, the method adopted in this research program for generating an impact load on a soil surface below which a structure is buried is similar to a shock tube arrangement. It consists of rupturing a metal burst disc by increasing the air pressure behind it to send a pulse onto the soil surface. The impact generator apparatus used in the test program is shown schematically in Fig. 11. The aluminum rupture disc is scratched with a certain geometric pattern, determined by trial and error, so that it will burst in a prescribed manner in order to send a pressure pulse through the shaping ring and the shaping box onto the soil surface. The spatial distribution of the pressure impinging on the surface, which is governed by the scratch pattern, is measured by the dynamic stress gages to be described later. The magnitude of the peak dynamic pressure is governed by the thickness of the disc used and the air pressure employed to cause the bursting. Peak pressures up to 200 psi have been obtained, while rise times on the order of 1 msec are easily achieved. The impact generator produces reproducible results and performed flawlessly throughout the test program.

#### B. Dynamic Stress Gage

One of the most important factors influencing the behavior of a buried structure is the soil pressure acting on the structure. It is crucial to measure this pressure in order to provide the data to compare the model test data against any analytical results. Toward this end, considerable efforts were devoted on developing a dynamic stress gage to use in the test program.

The material used to construct the stress gage is polyvinylidene fluoride (PVDF) which has piezoelectric properties. The PVDF film used in the construction of these gages was supplied by Systron Donner Company and is 0.025 in. thick. A 0.5 in. by 0.5 in. sheet of this material is cut out to act as the sensing element in the gage. The two

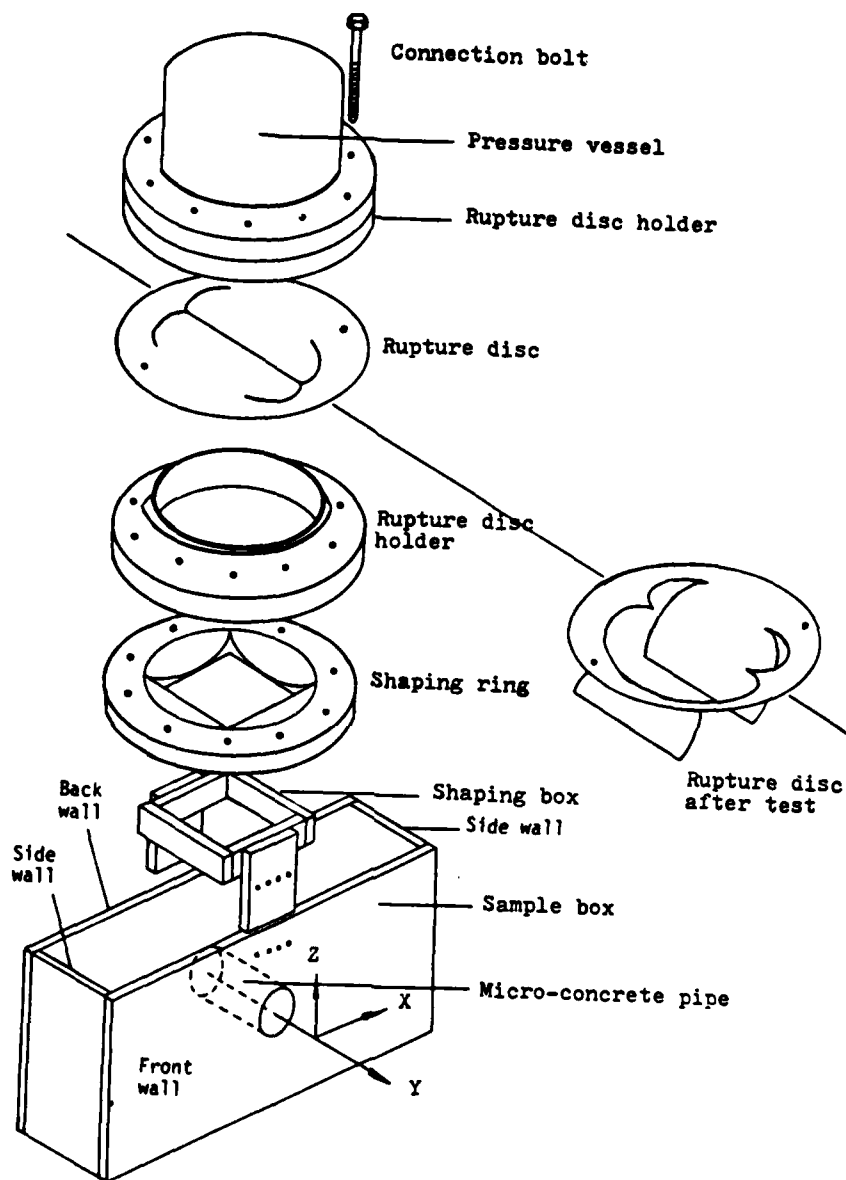
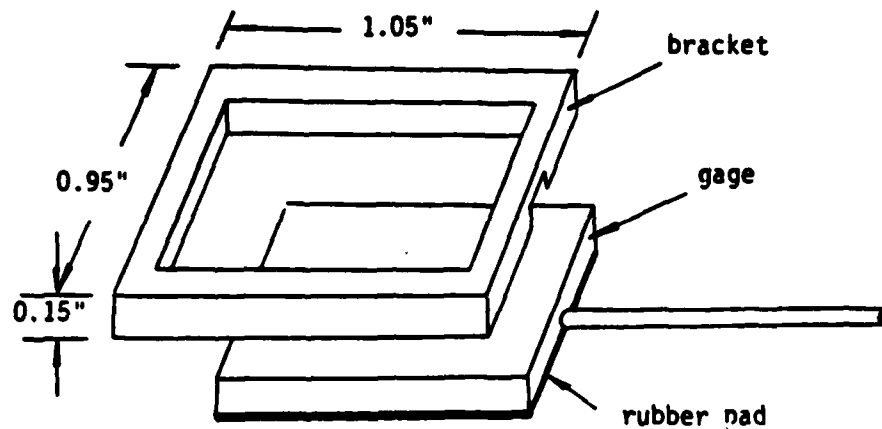
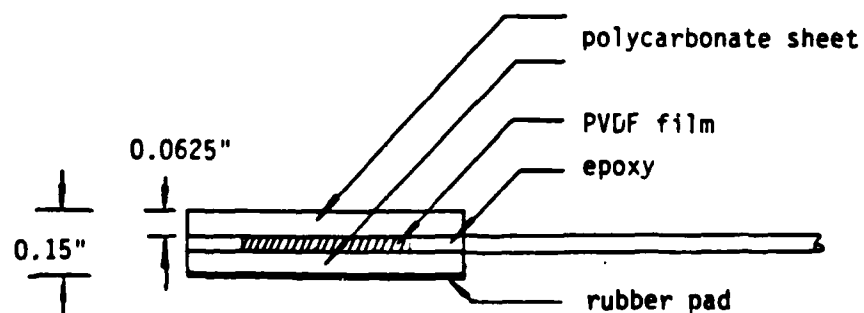
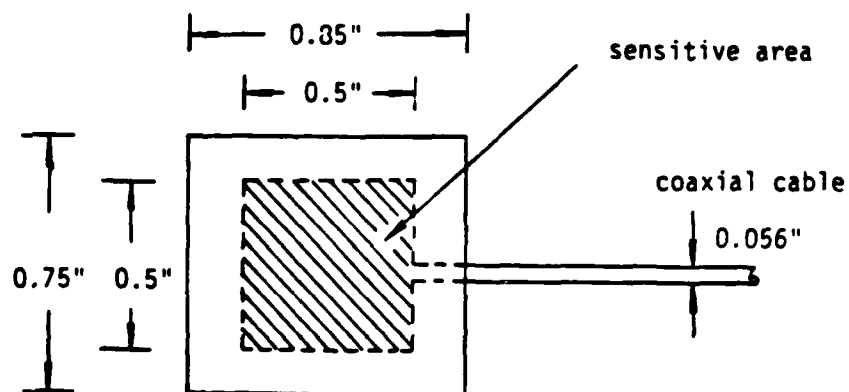


Figure 11. Expanded view of impact generator and centrifuge sample box

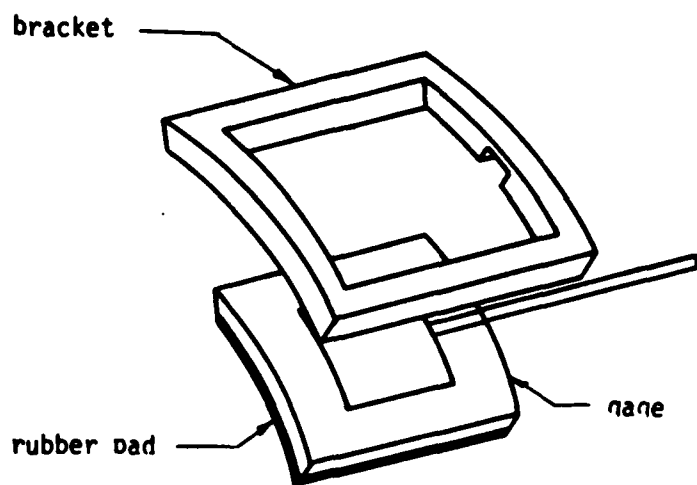


(a)

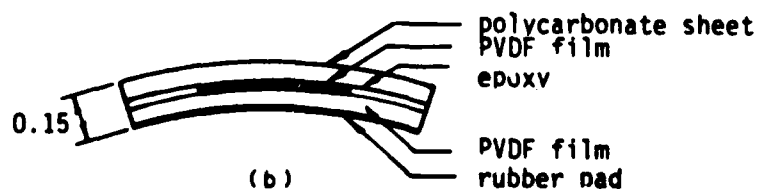
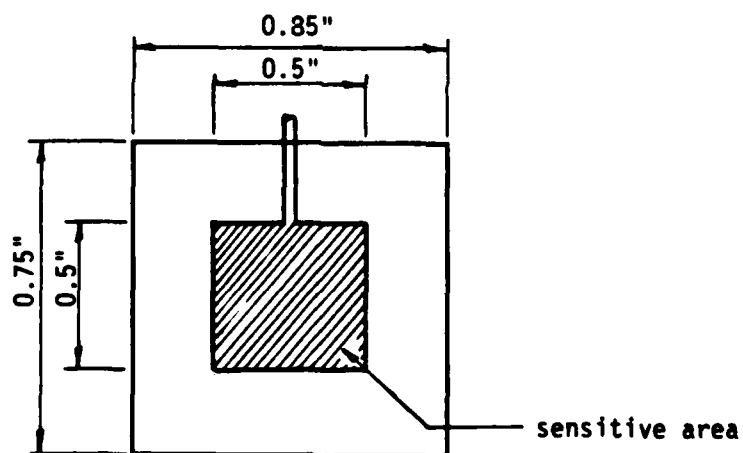


(b)

Fig. 12a. Schematic of Surface Stress Gage and Retaining Bracket.



(a)



(b)

Fig. 12b. Schematic of Contact Stress Gage and Retaining Bracket.

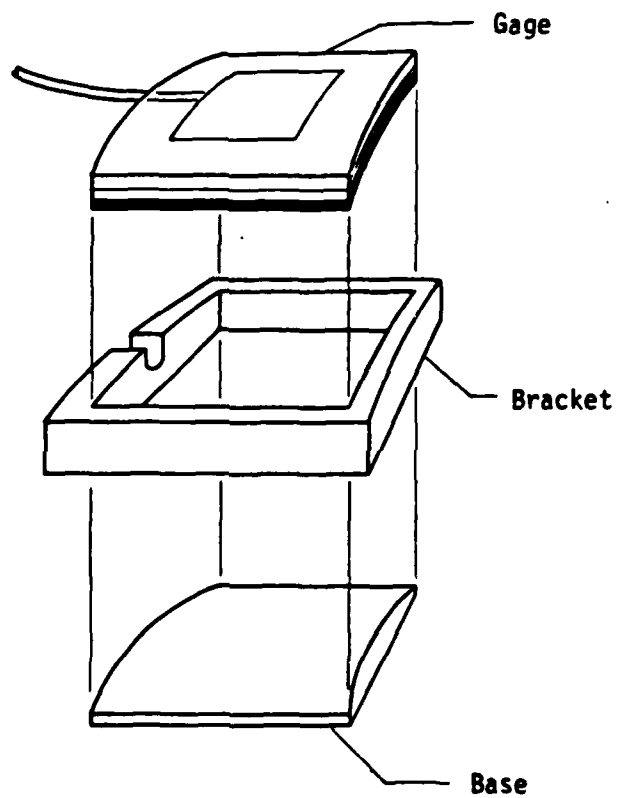


**Fig. 12c. Schematic of the Modified Free-Field Stress Gage and Retaining Bracket.**

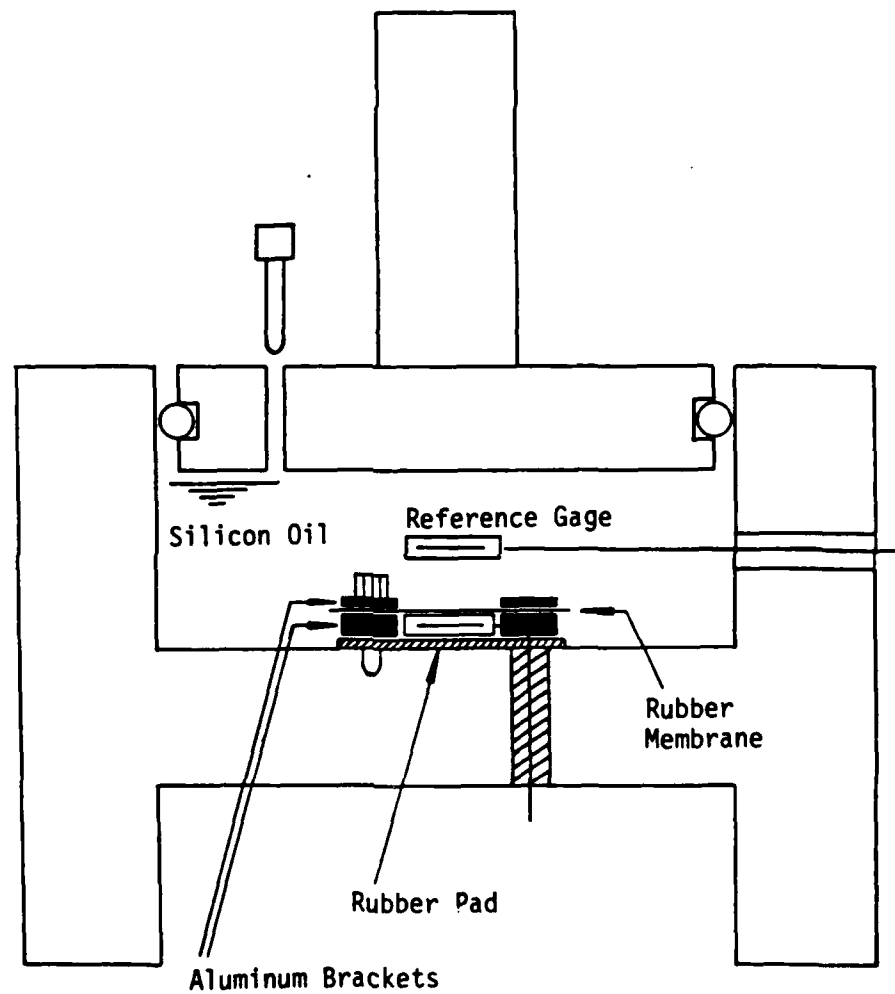


Figure 13a. Calibration of surface stress gage under 1-D loading

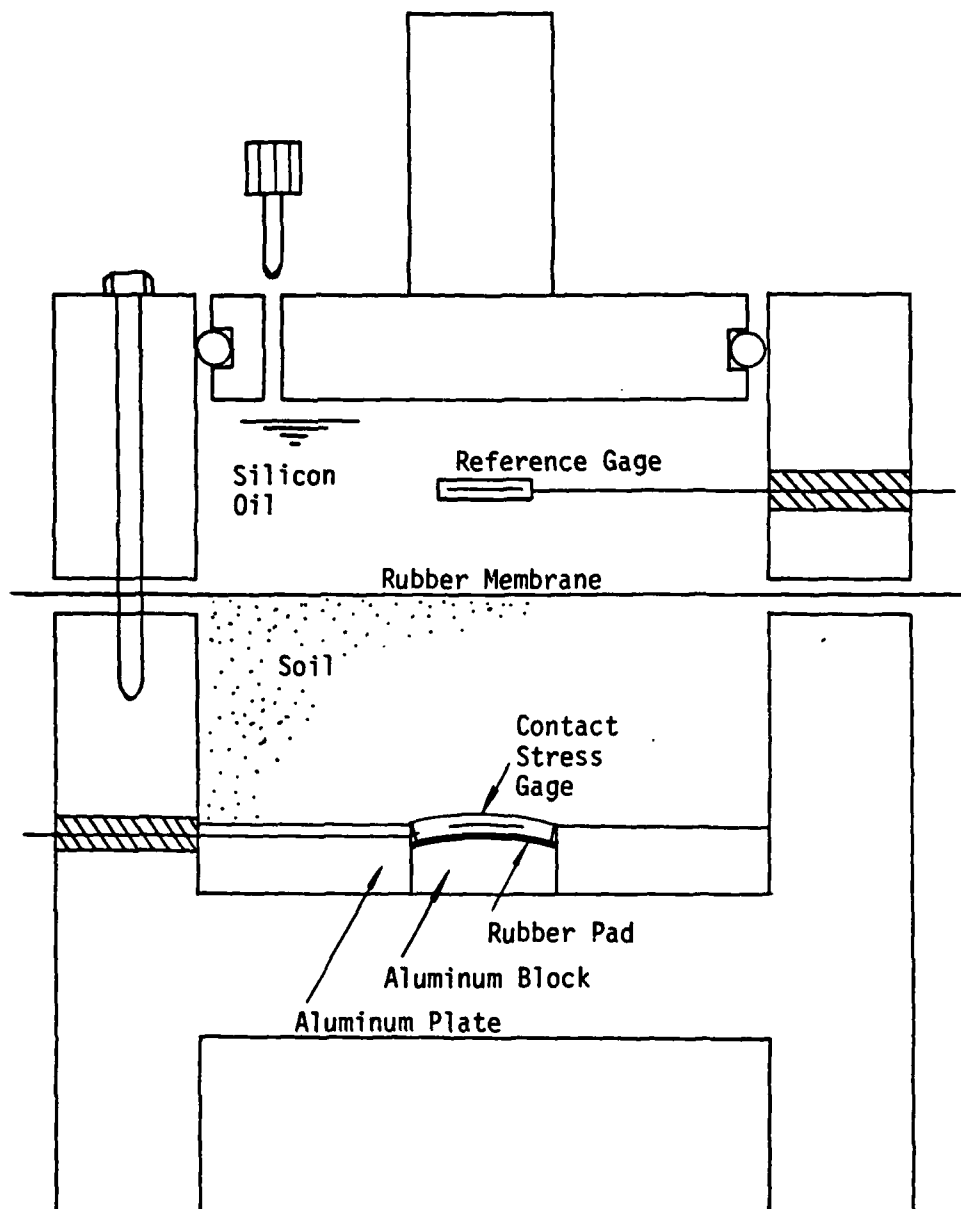


Figure 13b. Calibration of contact stress gage

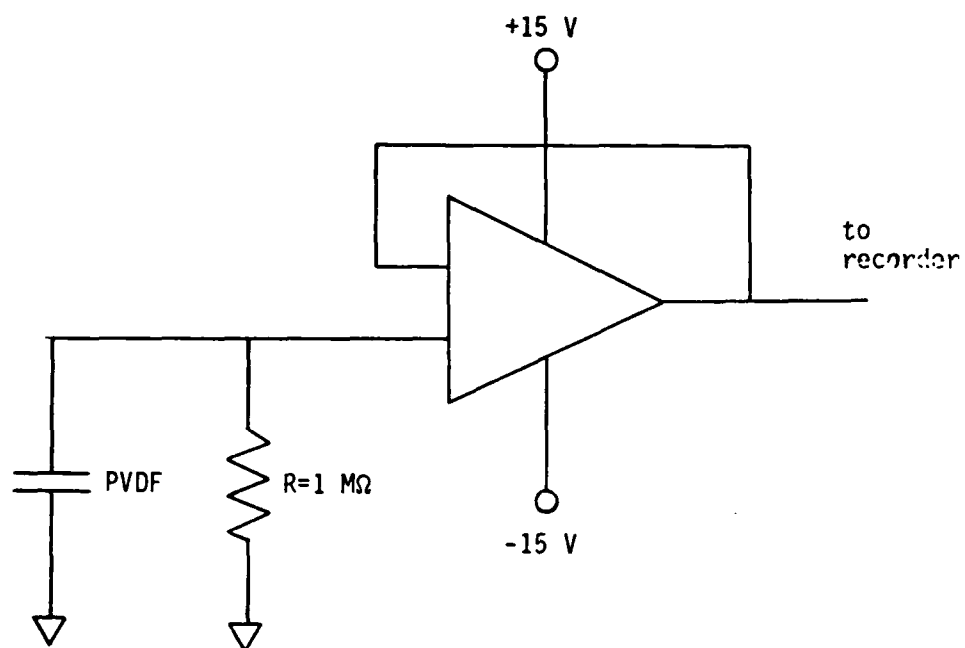


Figure 14. High impedance amplifier for dynamic stress gage

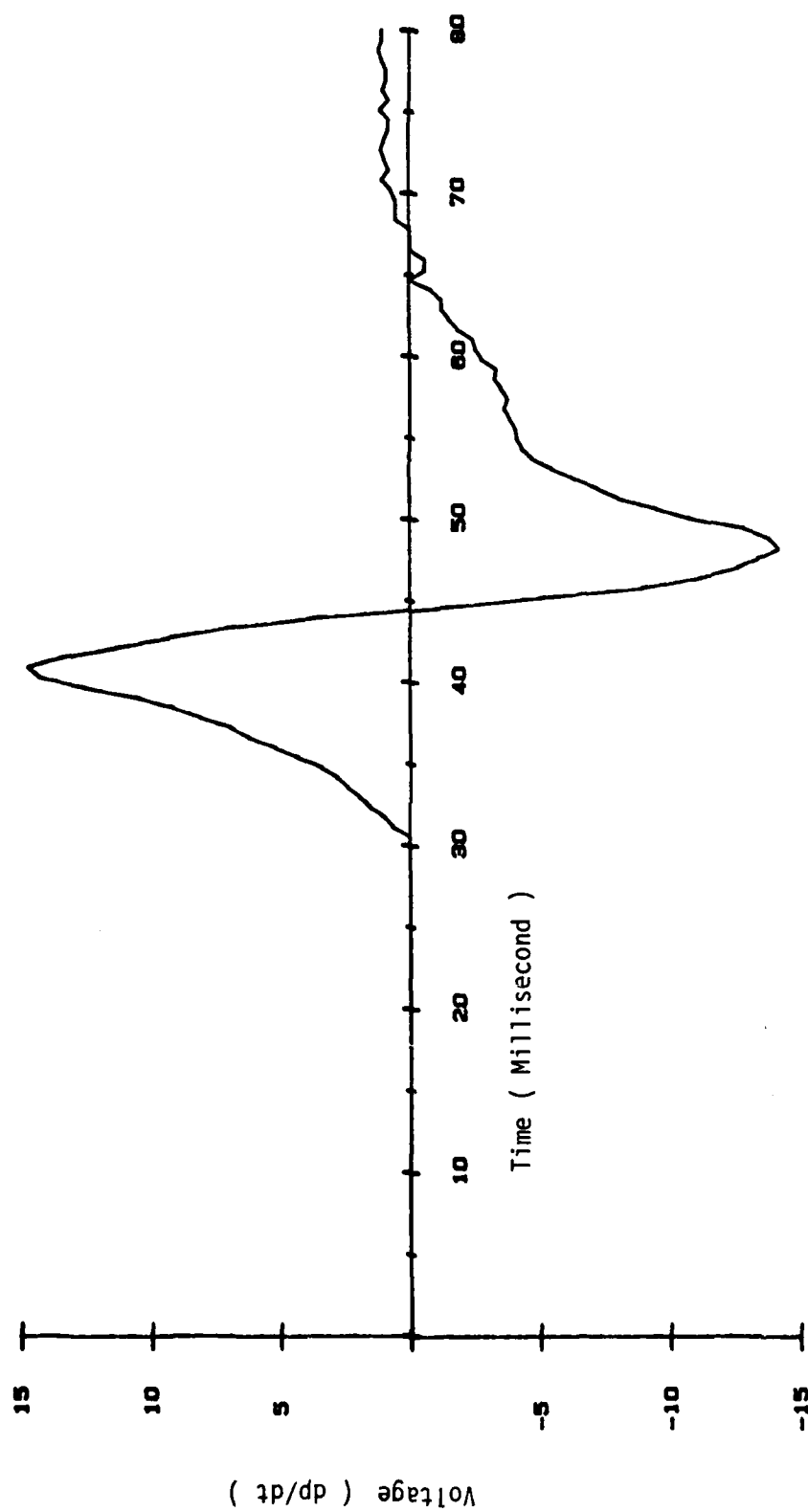


Figure 15a. Unintegrated dynamic stress gage signal, test 1SGPT.3D

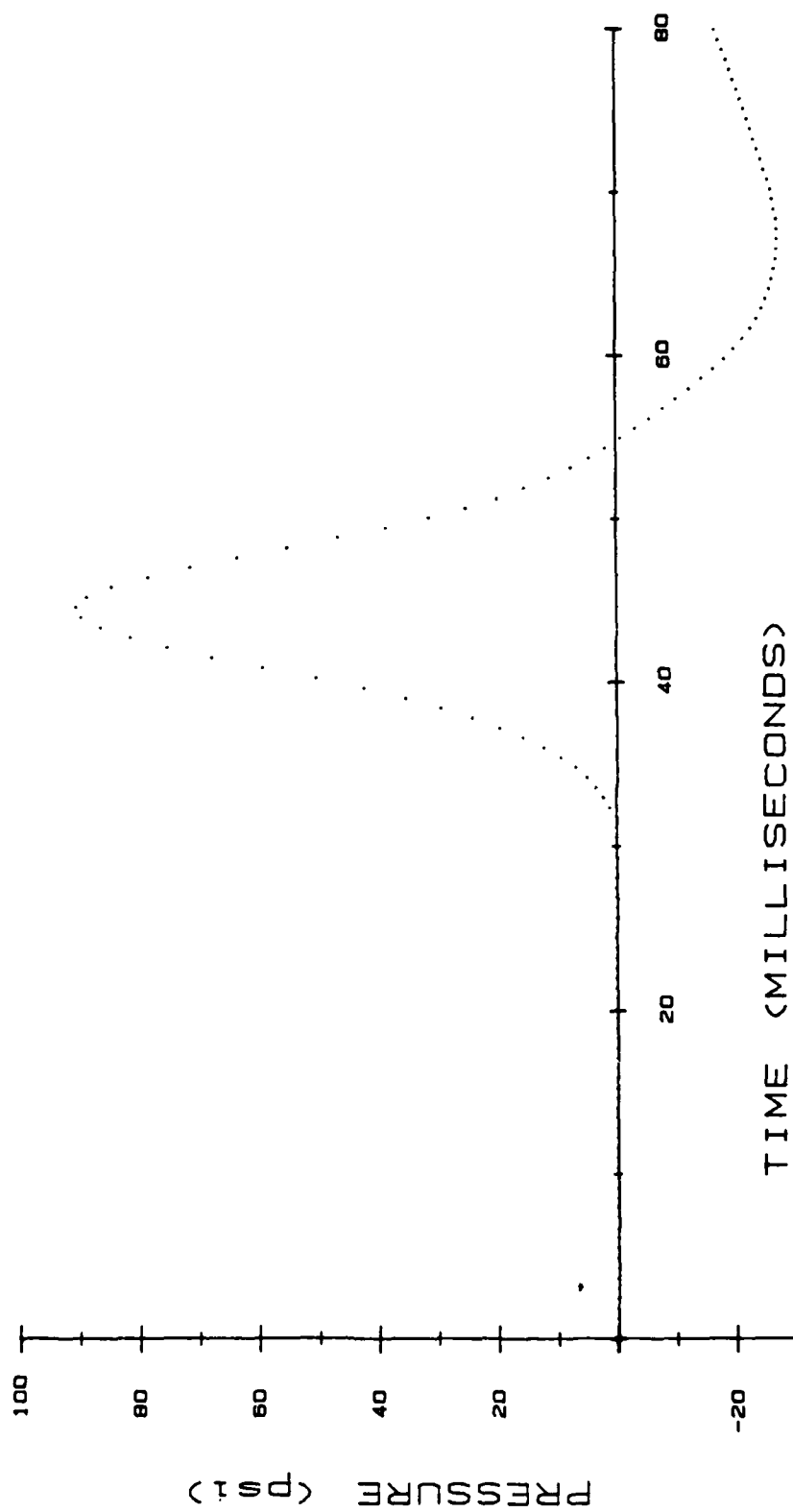


Figure 15b. Integrated, uncalibrated gage output

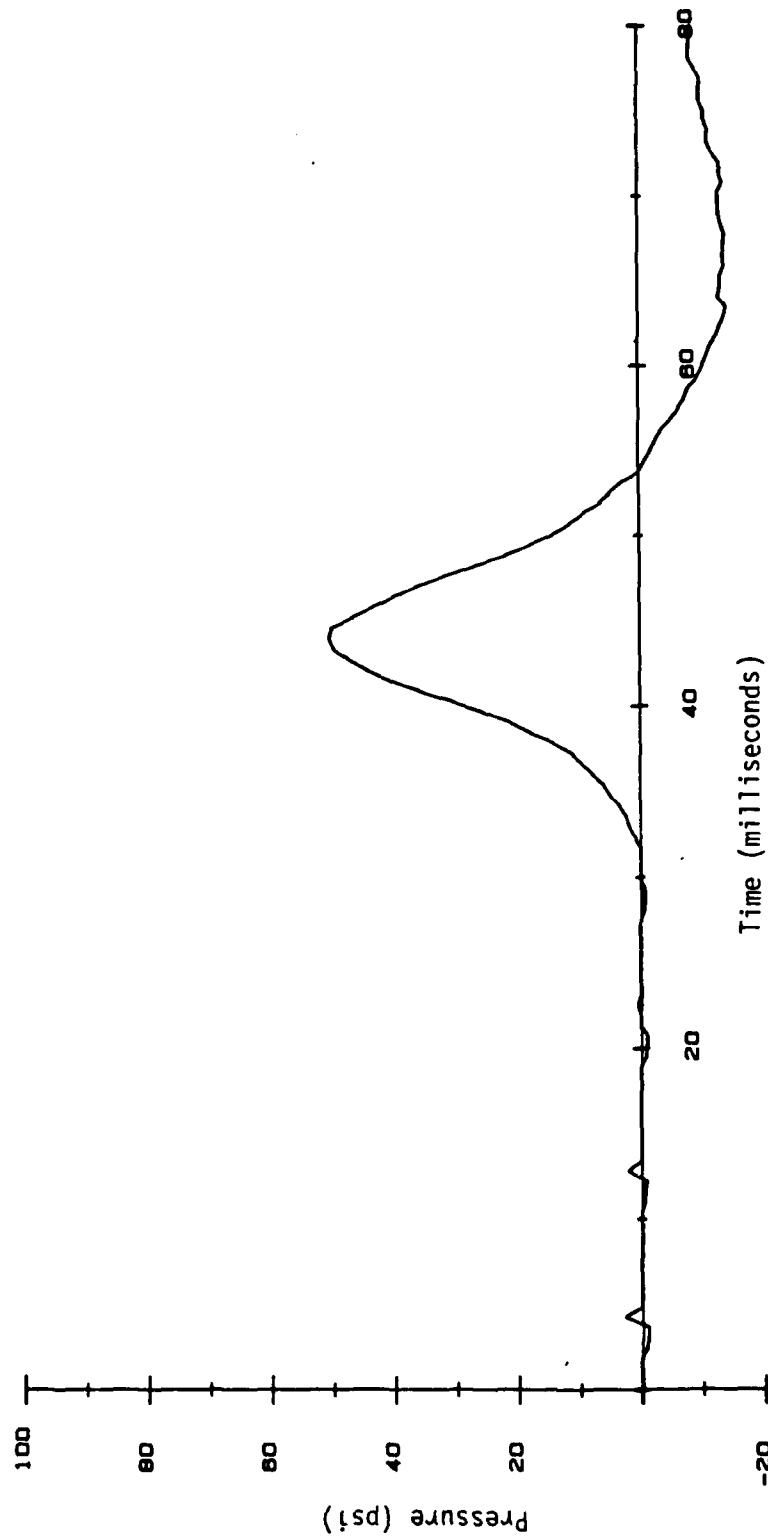


Figure 15c. Pressure transducer output

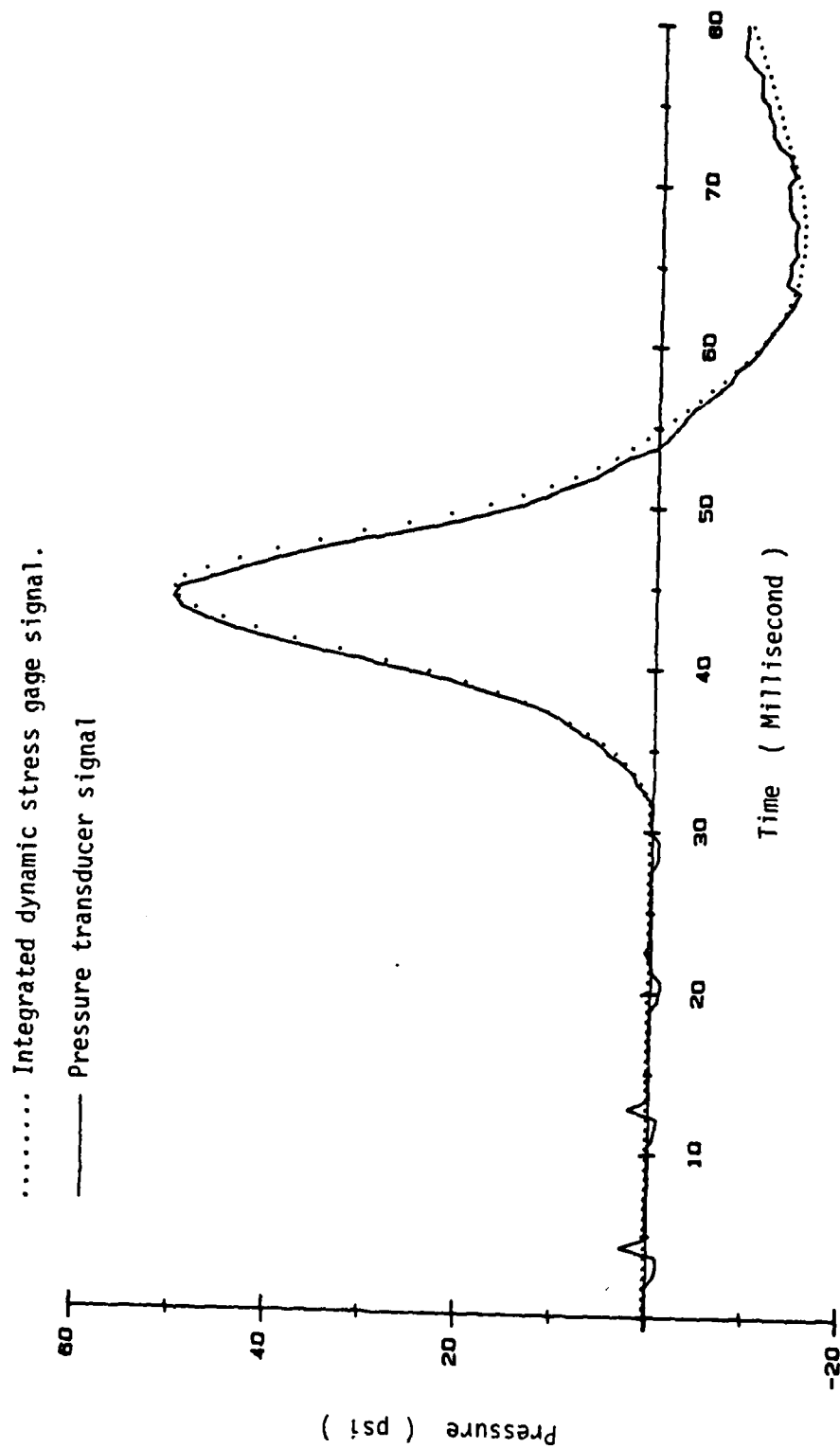


Figure 15d. Calibration of dynamic stress gage, test 1SGPT.3D

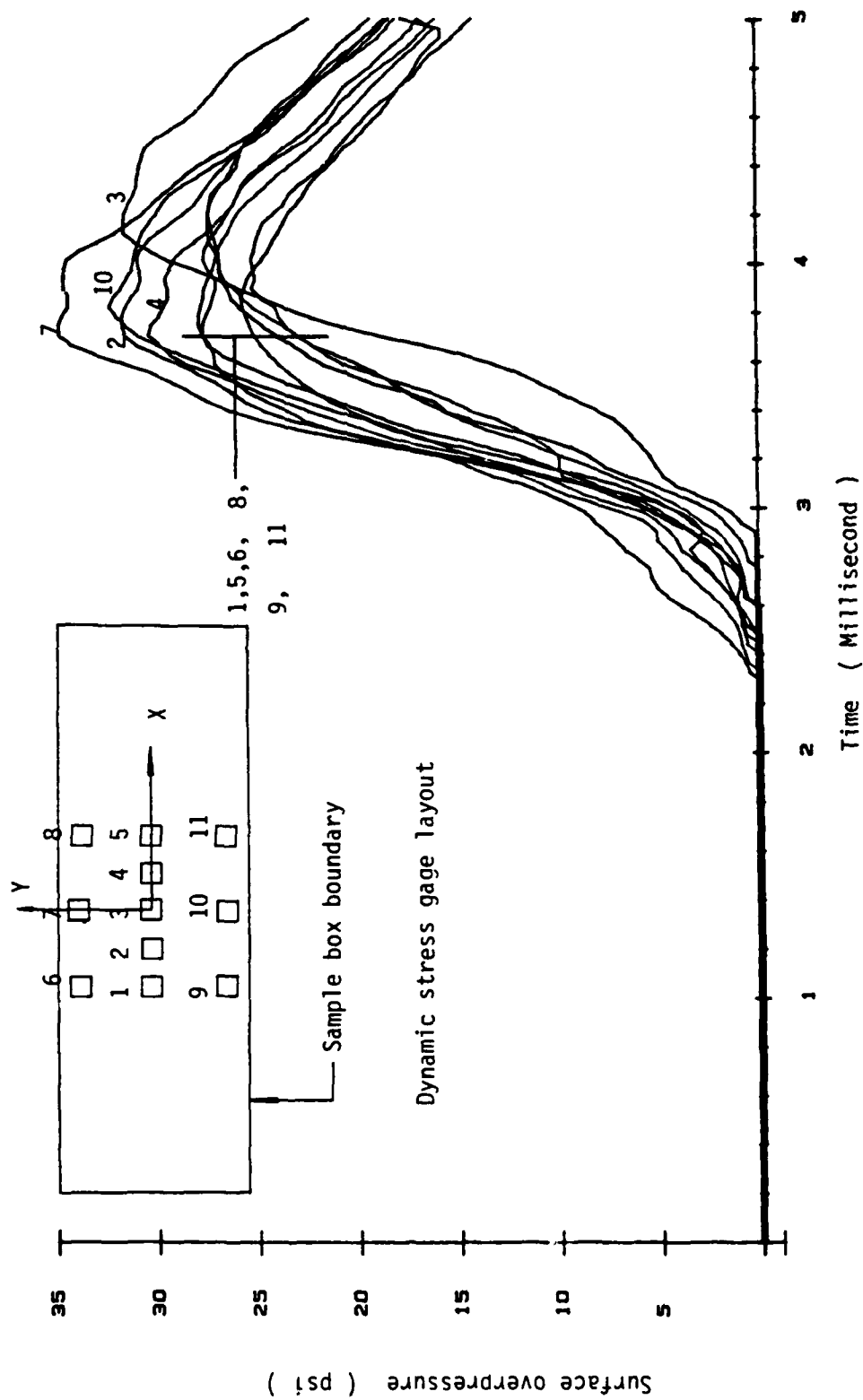


Figure 16. Measurement of surface overpressure distribution, test 12PCSG

surfaces of this sensing element are connected to a coaxial cable. The PVDF sheet is then covered by polycarbonate sheets on both sides for protective purposes and the sandwich assembly is then inserted into a retaining bracket that serves the purpose of isolating the sensing element from the effects of lateral stresses. In this fashion, only the normal stress acting on the sensing element will produce a signal from the gage.

Three versions of the gage have been developed, the first one for measuring the surface airblast pressure, the second for measuring the contact pressure on the pipe, and the third for measuring the free field stresses transmitted through the soil. They are shown schematically in Fig. 12. These gages were calibrated by using a calibration chamber as shown in Fig. 13, in which the conditions experienced by the gages in the centrifuge experiments were duplicated.

The gage was wired up in a circuit with a high impedance amplifier as shown in Fig. 14. The output from this circuit was recorded on a magnetic tape recorder and represented the rate of change of the pressure history acting on the sensing element in the gage, as shown in Fig. 15a. This signal was integrated digitally when the tape was played back for data analysis to produce the trace shown in Fig. 15b, which was then compared with the pressure history recorded by the pressure transducer in the calibration chamber shown in Fig. 15c. The comparison shown in Fig. 15d then established the calibration constant of the gage.

The surface stress gages were used to measure the distribution of the airblast pressure on the surface of the soil. A typical record is shown Fig. 16. The measurements obtained indicates that a uniform distribution exists in the y-direction while it is symmetrically distributed about the yz-plane. This justifies the assumption that a symmetrical plane strain situation exists in the centrifuge experiments, which would considerably simplify the analyses to be conducted of these tests later on.

### C. Micro-concrete Development

Because of the length scale reduction in centrifuge model testing, it would be futile to employ ordinary Portland cement concrete to construct the test models. A substitute material needs to be developed that has smaller aggregate sizes and which still retains the characteristics of concrete. A micro-concrete was developed for the test program in this project which satisfied these requirements.

This micro-concrete was manufactured by mixing 1 part gypsum (U. S. Gypsum Ultracal #60) to 0.8 parts sand (No. 20

Sieve) and 0.35 parts water. Since this mixture had a shelf life of only 15 minutes before setting, it was immediately poured into a mold for making the concrete pipe model. After 24 hours, the mold was stripped and another 24 hours later the concrete model was coated with shellac to prevent further curing of the gypsum as well as to keep moisture out of the micro-concrete.

Tests performed on cylindrical specimens of this micro-concrete materials showed that it has properties very similar to Portland cement concrete, with an unconfined compressive strength of 4,500 psi and a tensile strength of 530 psi.

#### D. Centrifuge Test Program

The principal set of centrifuge experiments were conducted by applying an airblast loading to the test model buried in a sand. The model was 4-in. in diameter and was buried horizontally in the soil sample. In this test series consisting of 24 experiments conducted at 50 g, the parameters varied were the relative stiffness between the soil and the structure which was influenced by the relative density of the soil as well as the thickness of the pipe, the magnitude of the blast loading and the depth of burial of the pipe. The test matrix for this part of the program is shown in Table 1. In addition to these centrifuge experiments, several tests on the buried pipe were also carried out under normal gravity in order to ascertain the difference in the two types of tests. In all tests on buried pipes, the instrumentation consisted of contact stress gages put on the outside surface of the pipe at five locations on one side of the vertical diameter: crown, 45° shoulder position, springline, 45° haunch position and invert. In addition, proximity transducers were mounted on a strong rod running on the inside of the pipe and mounted on the walls of the soil model container for measuring the deflections of the pipe at the crown, springline and invert. A surface stress gage was placed on the soil surface to record the magnitude of the airblast. All signals were recorded on a magnetic tape recorder, which were later played back for digitization and data analysis.

In analyzing the centrifuge test data, it was found necessary to also conduct tests on just the soil model without any buried pipes. In these "free-field" tests, stress gages were buried in the soil for measuring the magnitude of the stresses transmitted through the soil without interference from the presence of the buried pipe. The locations of the stress gages in these free-field tests corresponded to the crown, springline and invert locations of the contact stress gages in the buried pipe tests. Airblast loading of different magnitudes were employed,

Table 1. Test Matrix for Soil-Structure Interaction Experiments.

		Diameter to Thickness Ratio (D/t)														
		20.0			13.3			10.0			6.6			5.0		
Depth of Burial (Measured to crown)	Relative Density	70	85	90	70	85	90	70	85	90	70	85	90	70	85	90
2.0"	B															
	A						CF <sub>6</sub>									
	D			CF <sub>21</sub>			CF <sub>8</sub>			CF <sub>24</sub>			CF <sub>15</sub>			CF <sub>13</sub>
4.0"	C									CF <sub>20</sub>			CF <sub>16</sub>			CF <sub>14</sub>
	B												CF <sub>17</sub>			CF <sub>11</sub>
	A	CF <sub>23</sub>	CF <sub>22</sub>	CF <sub>4</sub>	CF <sub>2</sub>	CF <sub>3</sub>	CF <sub>1</sub>			CF <sub>9</sub>			CF <sub>10</sub>			CF <sub>12</sub>
6.0"	B															
	A							CF <sub>5</sub>								

Surface Pressure: A; 30-35, B; 45-50, C; 65-70, D; 95-110 (psi)

Surface Pressure: A; 30-35, B; 45-50, C; 65-70, D; 95-110 (psi)

Table 2. Test Matrix for Free-Field Experiments.

VERTICAL TESTS					HORIZONTAL TESTS					
Test #	Depth		D <sub>r</sub> (%)	P <sub>s</sub> (psf.)	Test #	Depth			D <sub>r</sub> (%)	P <sub>s</sub> (psf.)
	2" 4"	6"				4" 6" 8"				
1FFV	X	X	90	35	1FFL	X	X	X	90	45
2FFV	X	X	90	35	2FFL	X	X	X	90	33
3FFV	X	X	90	50	3FFL	X	X	X	90	78
4FFV	X	X	90	86	4FFL	X	X	X	90	102
5FFV	X	X	90	107	5FFL	X	X	X	90	36
6FFV		X	90	32	6FFL	X	X	X	90	35
7FFV		X	90	36	7FFL	X			90	25
8FFV	X		90	23	8FFL		X		90	20
9FFV		X	90	18	9FFL			X	90	22
10FFV		X	90	19	10FFL	X			90	36
11FFV	X		90	37	11FFL		X		90	38
12FFV		X	90	36	12FFL			X	90	37
13FFV		X	90	99	13FFL	X			90	80
14FFV	X		90	38	14FFL		X		90	89
15FFV		X	90	115	15FFL			X	90	84

duplicating the loadings used in the pipe tests. Thus, reference values were obtained for the in-situ stresses under airblast loading. These values were then used in defining the contact stress amplification experienced by the pipe at the corresponding location. Table 2 shows the test matrix for these free-field experiments

In analyzing the results of the buried pipe tests, it was found convenient to introduce a parameter called the contact stress ratio, CSR, which is defined as:

$$CSR = p_c / (NPSR) p_s \quad (1)$$

where  $p_c$  = peak normal stress measured on the pipe,  
 $p_s$  = peak surface pressure measured, and  
 $NPSR$  = normalized peak soil response  
 = peak free-field stress/peak surface pressure

Through this normalization, the variations arising from the different magnitudes of the airblast pressure are eliminated. CSR can also be considered as a "stress concentration factor" since it is defined in reference to the free field stress.

To incorporate the various thicknesses of the pipes that were tested in the program, a dimensionless structure-soil stiffness ratio, denoted as  $K_{ss}$ , is defined as:

$$K_{ss} = EI / M_s D^3 \quad (2)$$

where  $E$  = Young's modulus of the micro-concrete,  
 $I$  = moment of inertia of the pipe,  
 $M_s$  = constrained modulus of the soil, and  
 $D$  = diameter of the pipe.

Typical test results are shown in Figs. 17, 18 and 19, in which similar tests at 1 g and at 50 g are compared. It is seen that considerable differences were found in the behavior of the pipe in these tests. For instance, the deflections were much larger in the 1-g tests and the contact pressure distributions had different shapes. These differences can be attributed to the fact that the 50-g test was conducted in an environment in which the in-situ stresses around the pipe corresponded to a prototype situation where the pipe was buried at a depth 50 times larger than in the 1-g test. The increase in the overburden stresses in the 50-g test arising from the elevated gravity-induced self-weight loading obviously produced higher confinement which in turn led to smaller deflections. In addition, the larger stress gradient in the 50-g test, again due to the increased body forces produced in the centrifuge, also was responsible for the different contact stress distribution around the pipe. The conclusion is drawn from

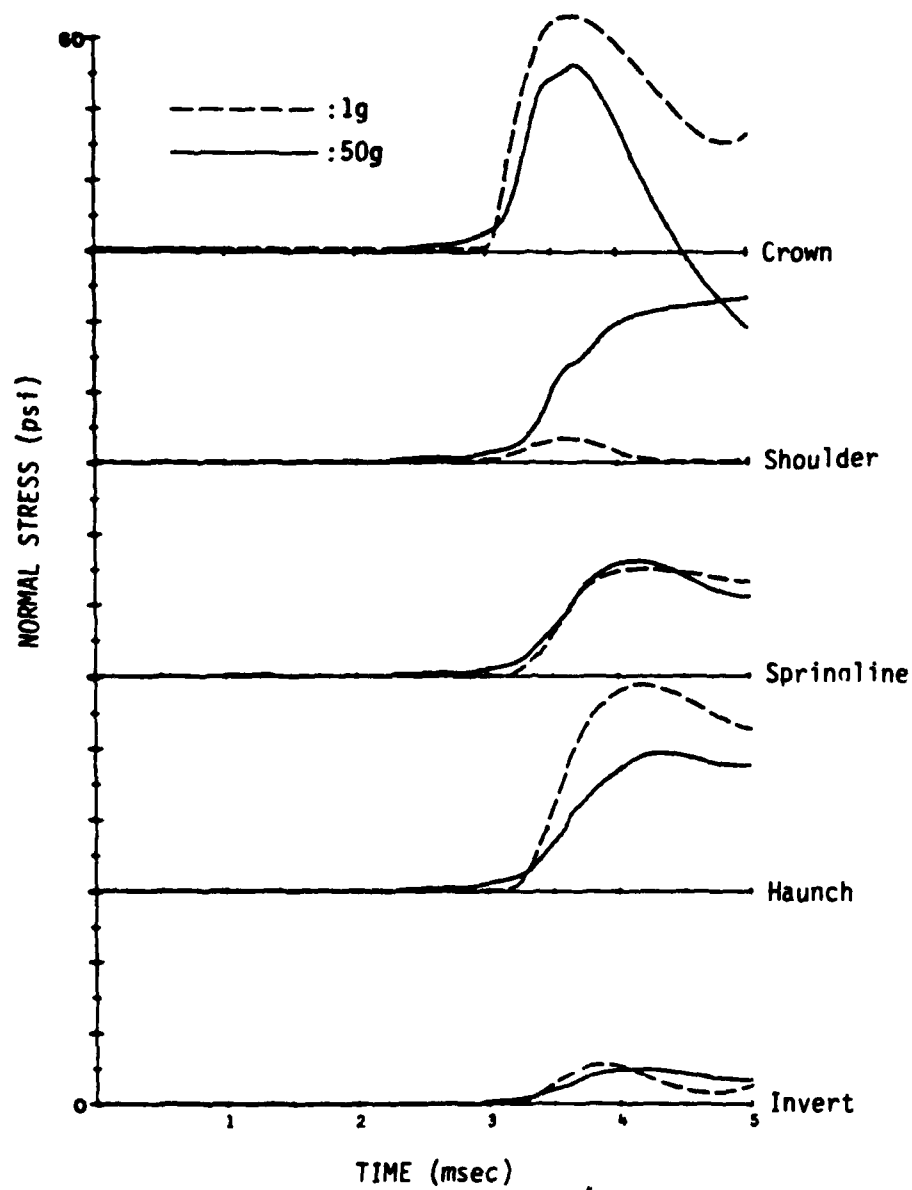


Fig. 17. Stress History Comparison for 1-g and 50-g Experiments.

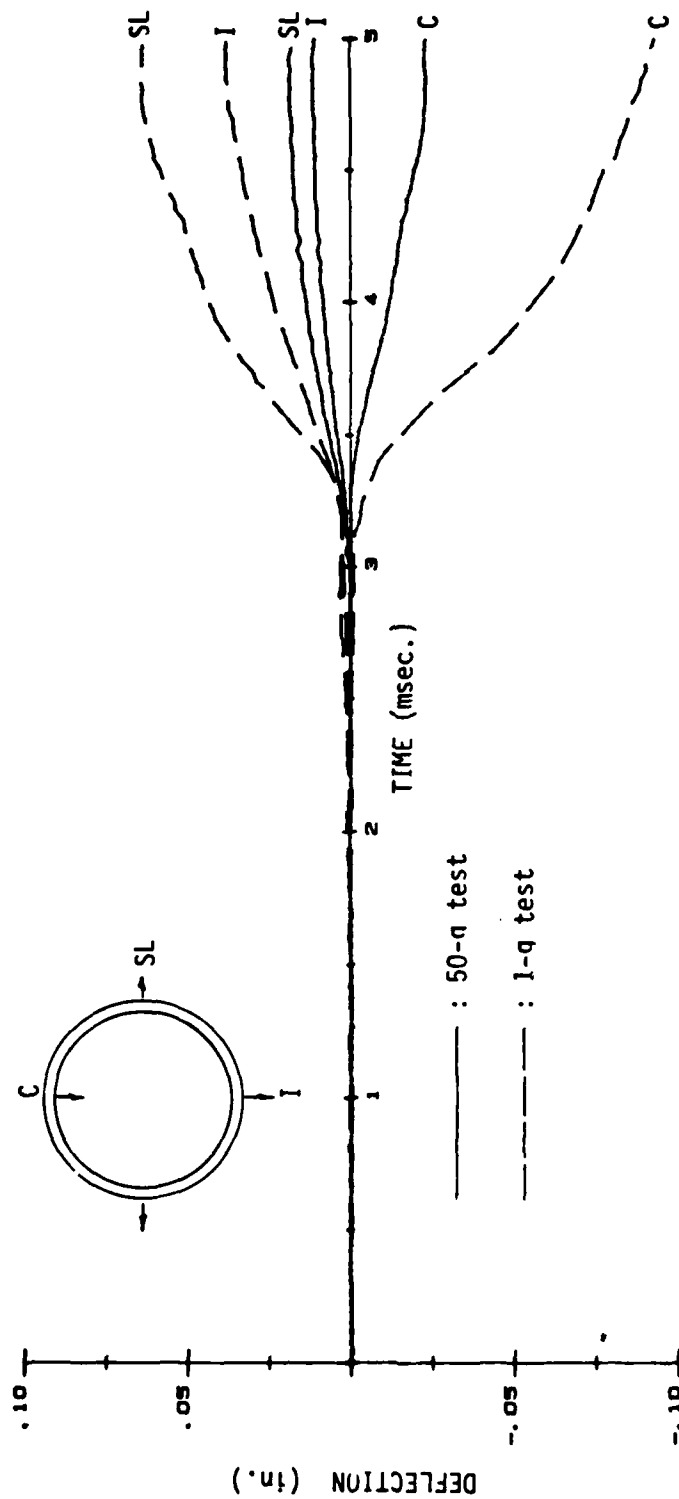
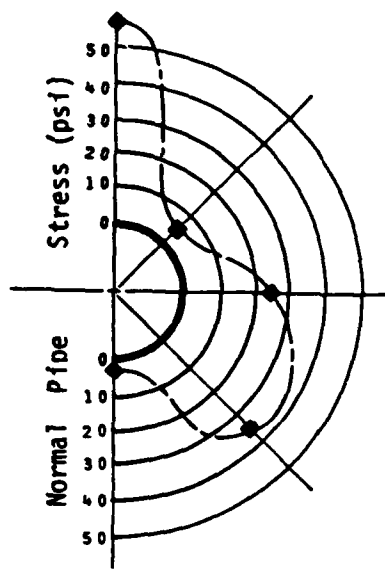
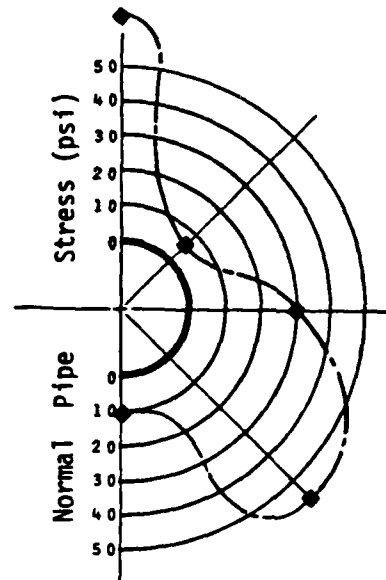


Fig. 18. Comparison of Pipe Deflection Histories for 1-g and 50-g Experiments.



Test 1N: 1-g

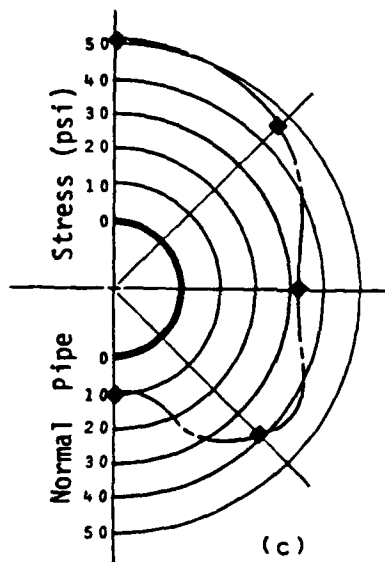
(a)



Test 2N: 1-g

(b)

Test CF1: 50-g



(c)

\*Note: Plotted are the peak contact stresses acting on the pipe.

Fig. 19. Pressure Distribution Comparisons for 1-g and 50-g Experiments.

this comparison that it is necessary to perform model tests at the correct simulation of the body force loading which is made possible by testing in the centrifuge.

The effect of the pipe stiffness on the response of the pipe is shown in Figs. 20, 21 and 22 for the CSR at the crown, springline and invert, respectively. The data in these figures show that at a structure-soil stiffness ratio  $K_{ss}$  of 100 or greater the CSR values measured remained constant, indicating that the pipe can now be considered to be "rigid". The change in the CSR values for pipes with  $K_{ss}$  less than 100 is due to the flexibility of the pipe, which caused different degrees of interaction with the surrounding soil. These interactions can also be displayed by plotting the pressure distribution around the pipe, as shown in Fig. 23. Here, as diameter to thickness ratio ( $D/t$ ) of the pipe decreased the pressure distribution changed substantially. As the pipe became more rigid, the crown and invert pressures increased while the springline pressure decreased. This is obviously the result of reduced deflections experienced by the more rigid pipes.

The effect of the intensity of airblast loading on the pipe response is shown in Fig. 24 for the crown contact stress ratio. Bearing in mind that the CSR is already a normalized parameter, the decrease of its value as the surface pressure increased indicated that there are nonlinear effects present in the soil-structure response. Since the micro-concrete material is essentially linearly elastic up to the point of failure, the nonlinearity exhibited in Fig. 24 could only be due to the soil. In Eq. 2, the constrained modulus  $M_s$  of the soil is represented in the definition of  $K_{ss}$ .  $M_s$  is certainly not constant and increases as the pressure level increases. Thus, the pipe would appear as more flexible as the surface pressure level increases. Hence, the lower CSR values observed at higher surface pressures can be explained.

The effect of the relative density of the soil was also investigated. However, in the range of relative density investigated (70% to 90%), there was no discernible trend in the data. It is concluded that in this range of the relative density all pipes in the thickness range employed appear to be rigid.

#### E. Numerical Analysis

The finite element code, SAMSON2, used in the numerical analysis in this project was obtained from the U. S. Air Force Weapons Laboratory. SAMSON2 is a two-dimensional finite element code developed primarily for dynamic analyses of plane and axisymmetric solids. It is used mainly for analysis of blast types of loading such as those resulting

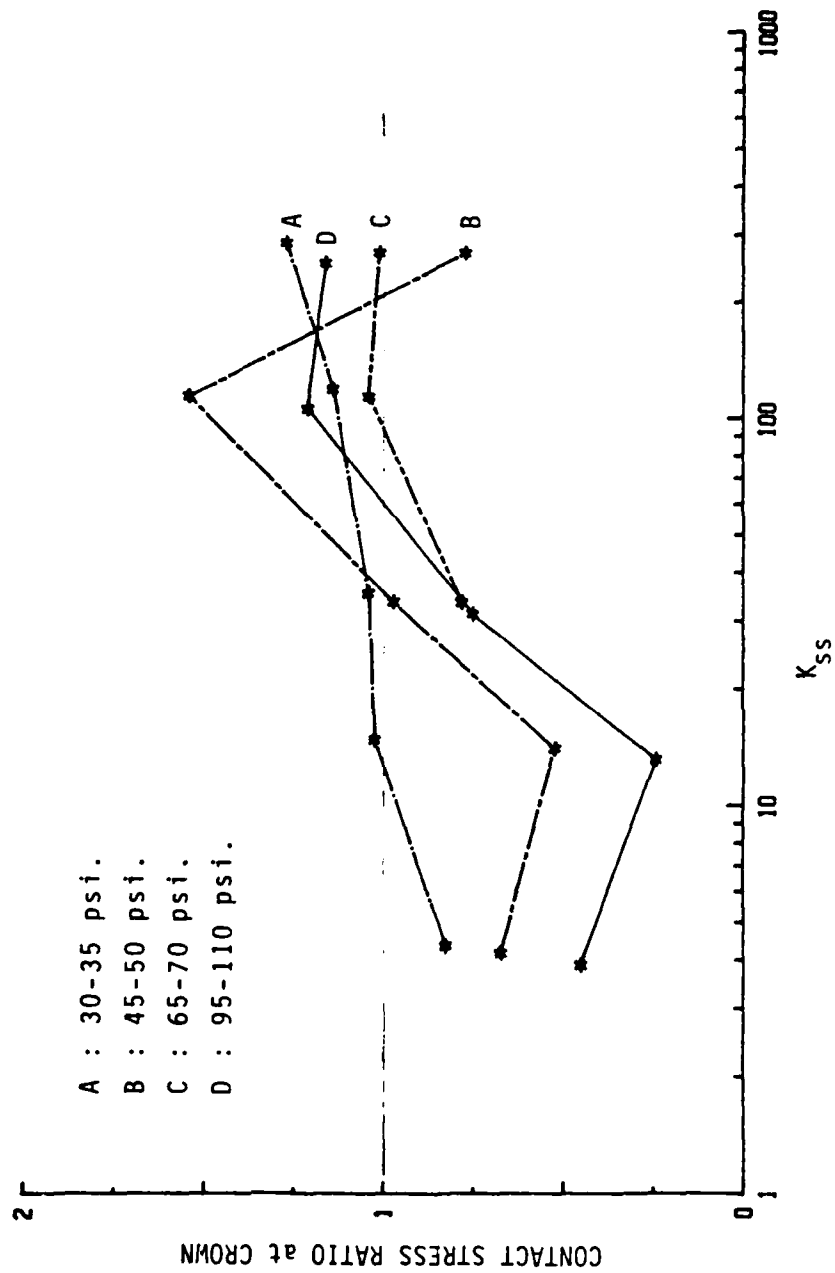


Fig. 20. Plot of CSR at Crown vs.  $K_{ss}$  for Various Surface Pressure Levels.

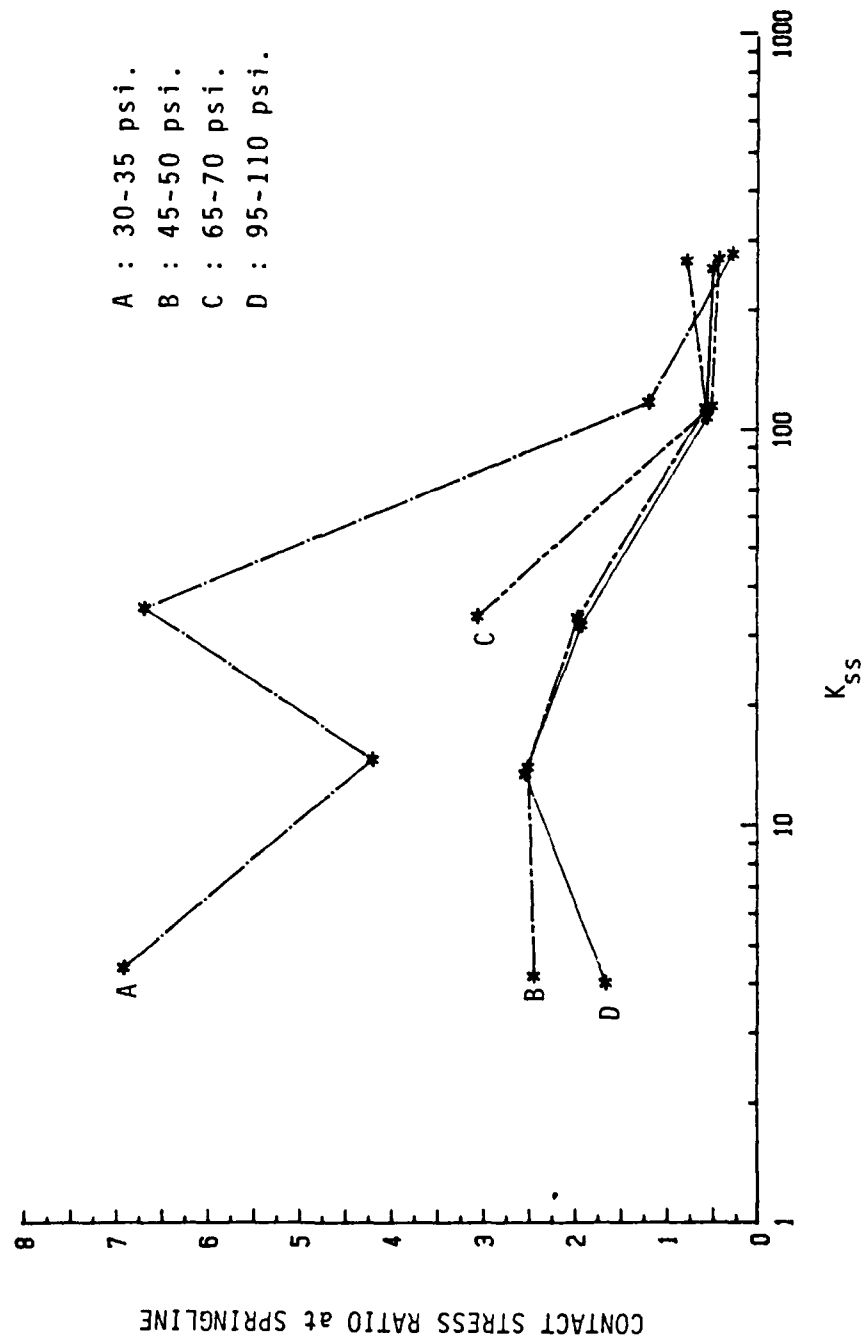


Fig. 21. Plot of CSR at Springline vs.  $K_{ss}$  for Various Surface Pressure Levels.

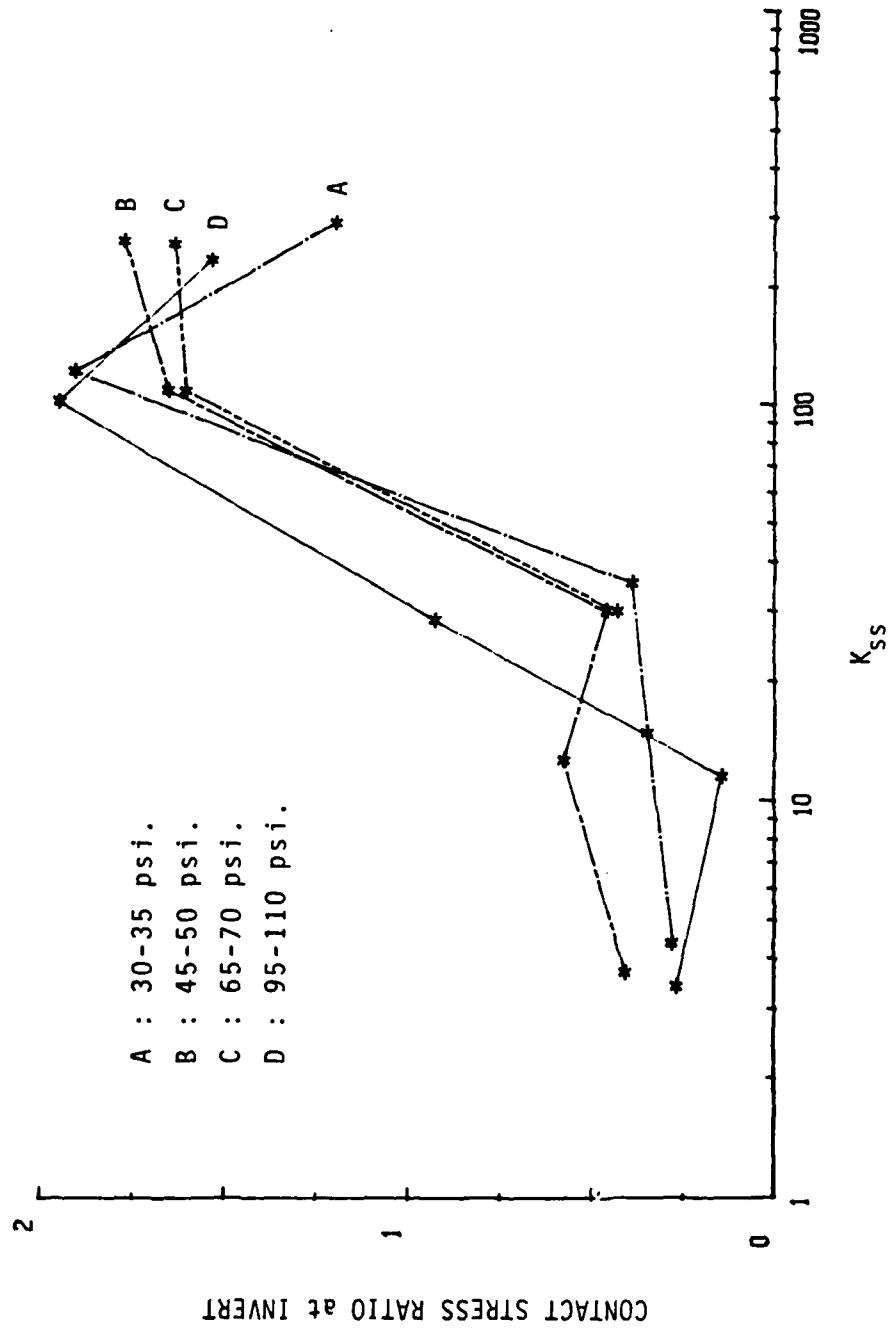


Fig. 22. Plot of CSR at Invert vs.  $K_{ss}$  for Various Surface Pressure Levels.

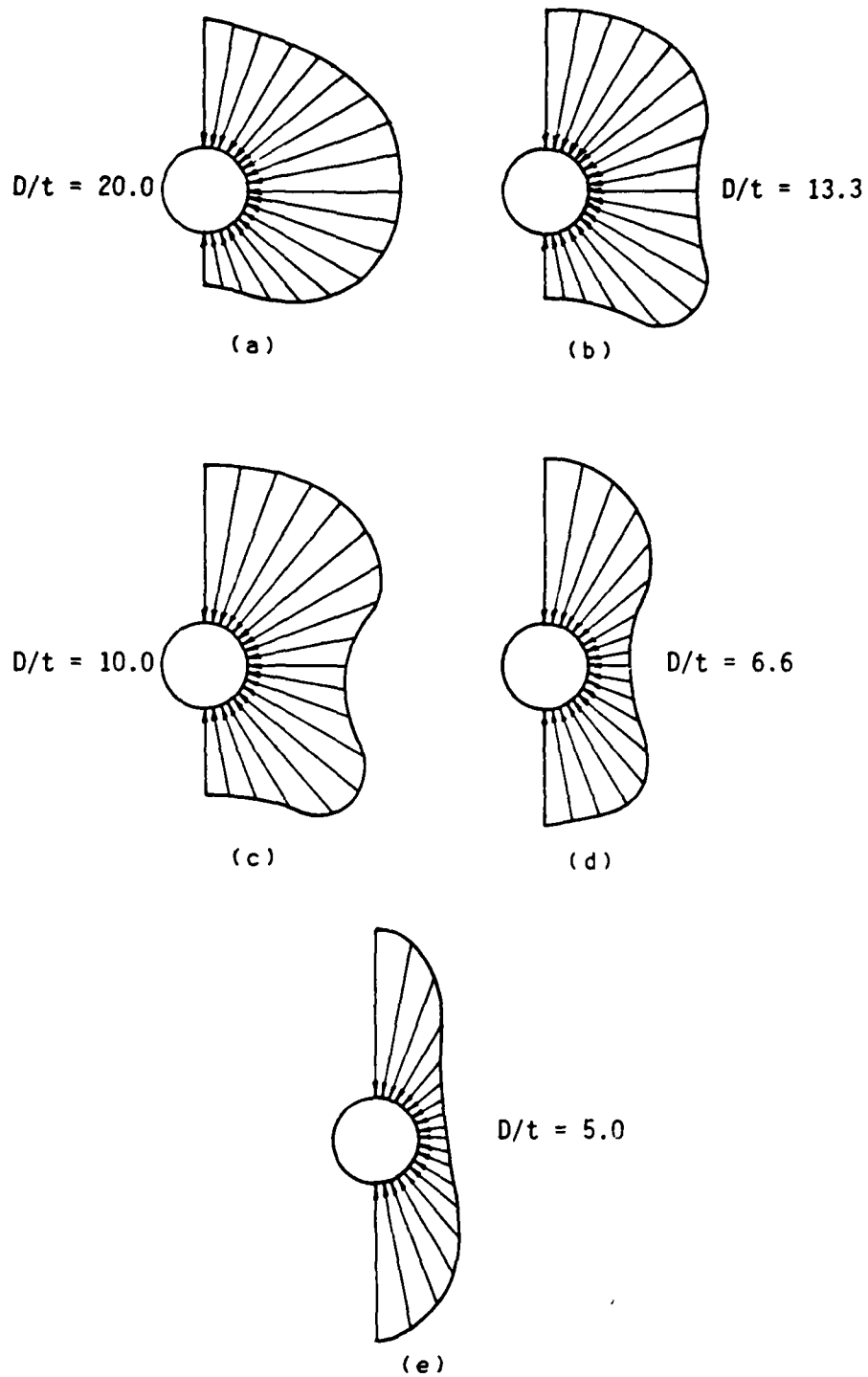


Fig. 23. Changes in Pressure Distribution with Respect to Pipe Stiffness.

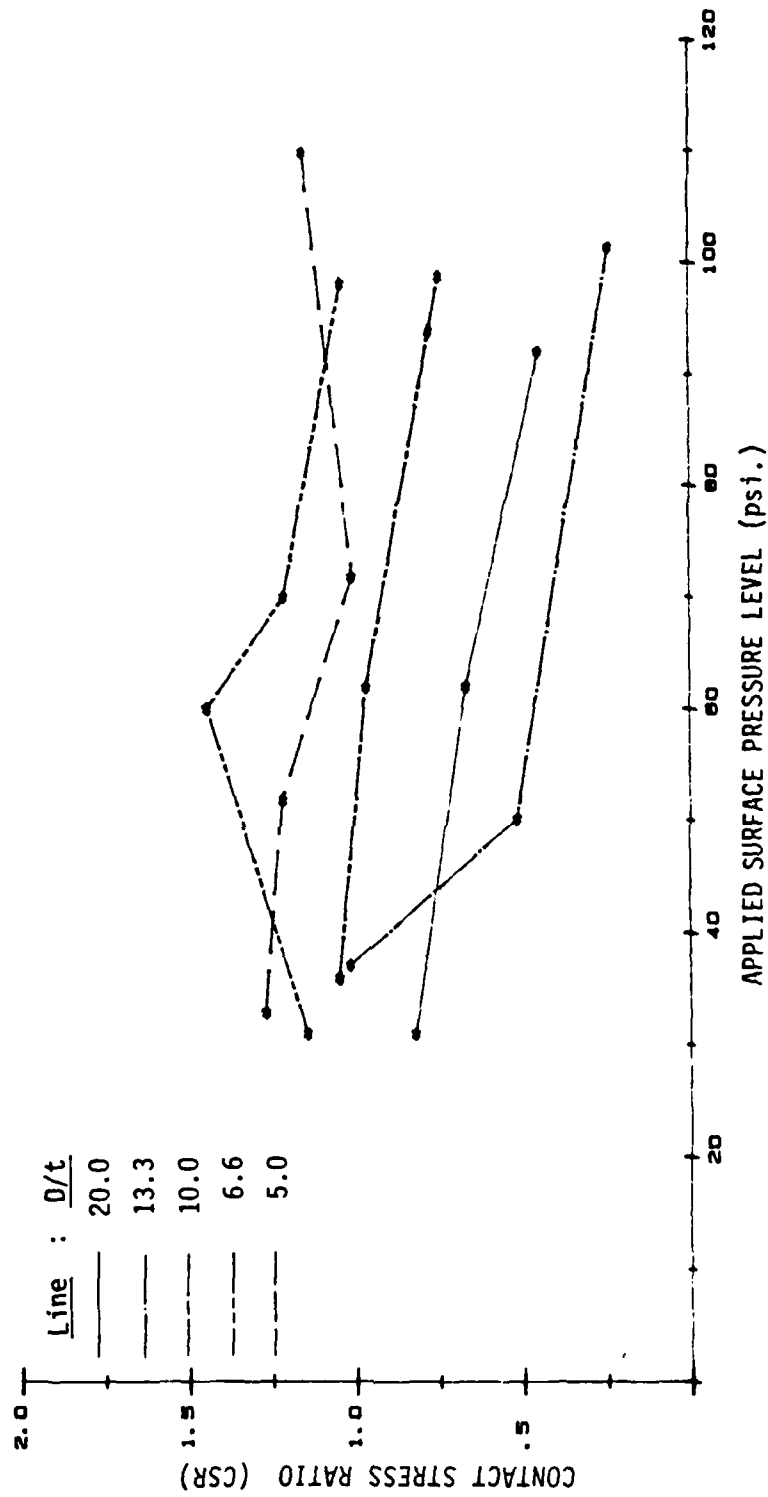


Fig. 24. Plot of CSR at Crown vs. Applied Surface Pressure Level.

from high explosives. The main features of the code include a central finite difference explicit time integration, an elasto-plastic cap model for the soil's constitutive properties, and the Air Force engineering model for concrete properties.

This code was chosen for this study because it was felt that, since it is being used by the Air Force in many engineering and development projects dealing with the analysis of soil-structure interaction under blast loading, it would be beneficial to ascertain its ability to correctly predict the performance of the buried pipes that were tested in the centrifuge environment where the in-situ conditions were properly simulated. Toward this end, this code was implemented in the Civil Engineering Apollo workstation computing network at the University of Colorado. The calibration of the constitutive models for the soil and the micro-concrete was carried out according to established procedures, using stress-strain properties determined by laboratory testing of the same materials as used in the centrifuge tests.

Both the free field tests and the buried pipe tests were analyzed by the SAMSON2 code. Fig. 25 shows the results of the free field analysis, by plotting the free field stress ratio (the maximum free field stress over the maximum applied surface overpressure) versus the maximum surface overpressure. Comparison is also made in this figure between the analytical values and the measurements at the crown position in the centrifuge tests. Excellent agreement is obtained for this comparison.

Typical centrifuge test results on buried pipes are shown in Fig. 26, showing the time histories of the surface overpressure as well as the contact stress measured at several points around the pipe. The results of the SAMSON2 analysis using a linear model for both soil and micro-concrete and a full nonlinear representation for both materials are compared with the experimental data in Fig. 27. Good agreement is observed for the contact stresses at all the locations analyzed.

Analyses were performed of the experiments that were conducted to investigate the effects of the structure-soil stiffness ratio. The comparison between experimental data and analytical results are shown in Figs. 28, 29 and 30, in terms of the contact stress ratio. Excellent agreement is again observed.

Although good results were obtained from using the SAMSON2 code, a word of caution must be recorded regarding its general utilization in dynamic analysis. The code is not unconditionally stable and convergence is not always

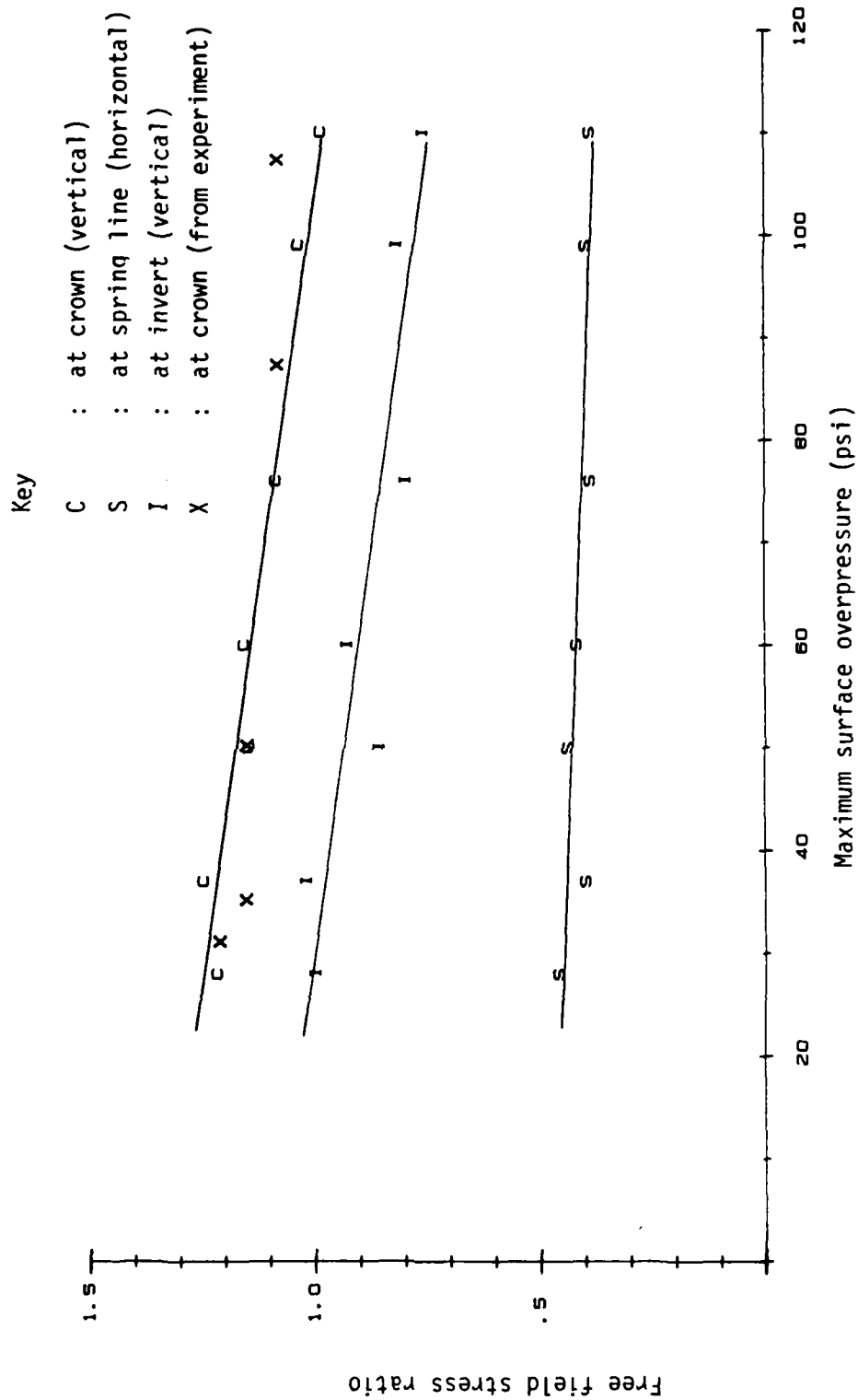


Figure 25. Plot shows stress ratio vs. maximum surface overpressure at different locations

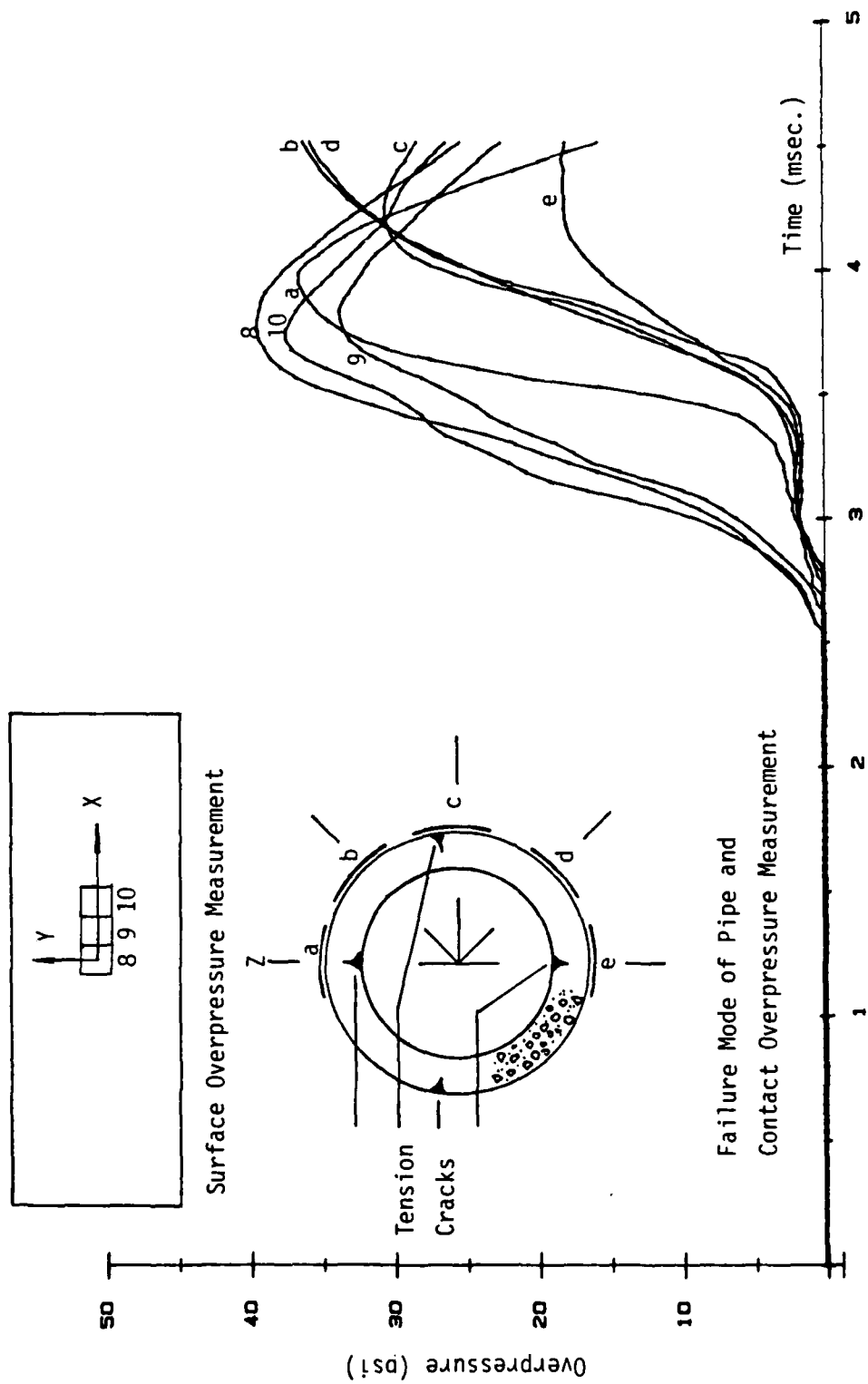


Figure 26. Summary of centrifuge test 1

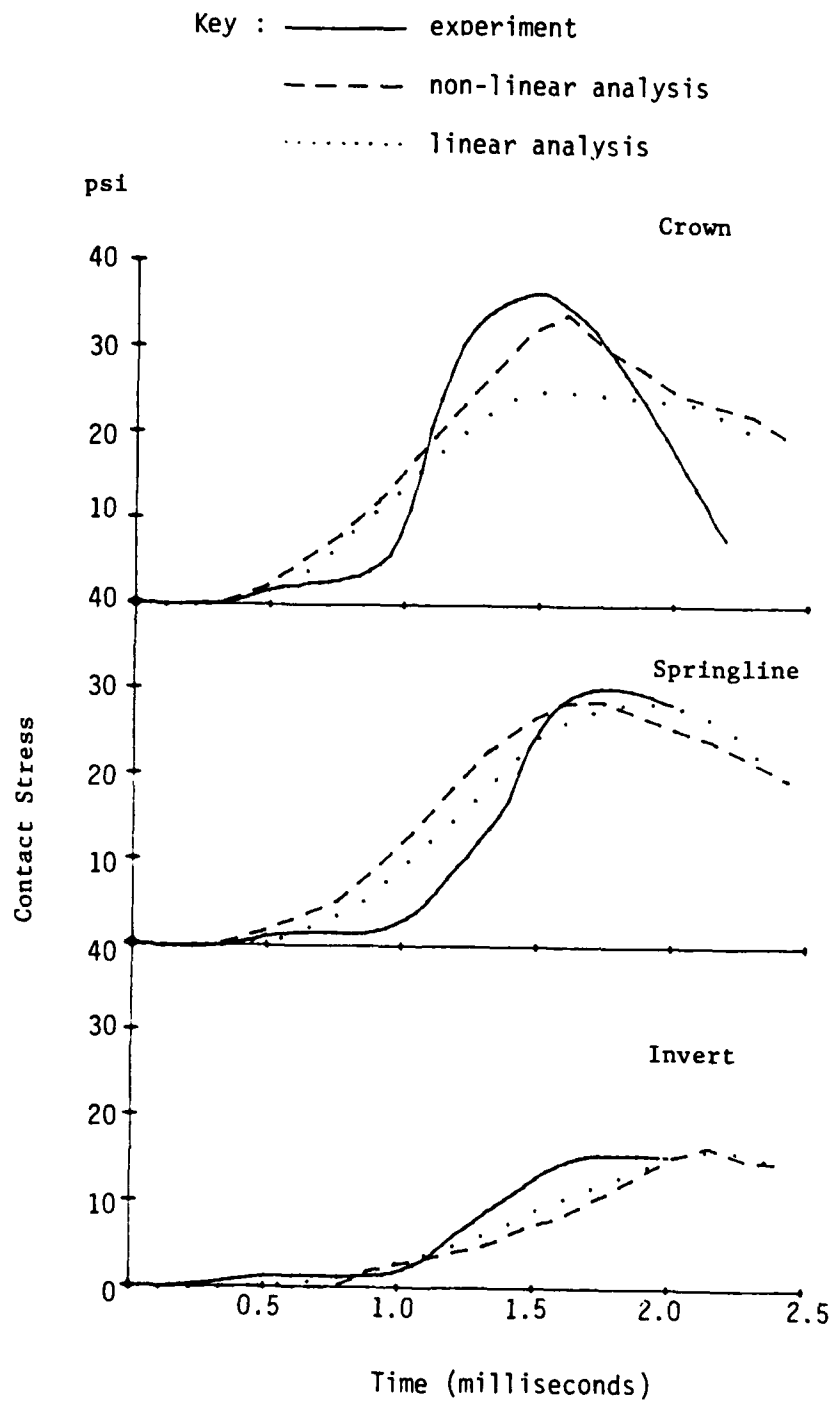


Figure 27. Comparisons between the experiment and the analyses. Test 1

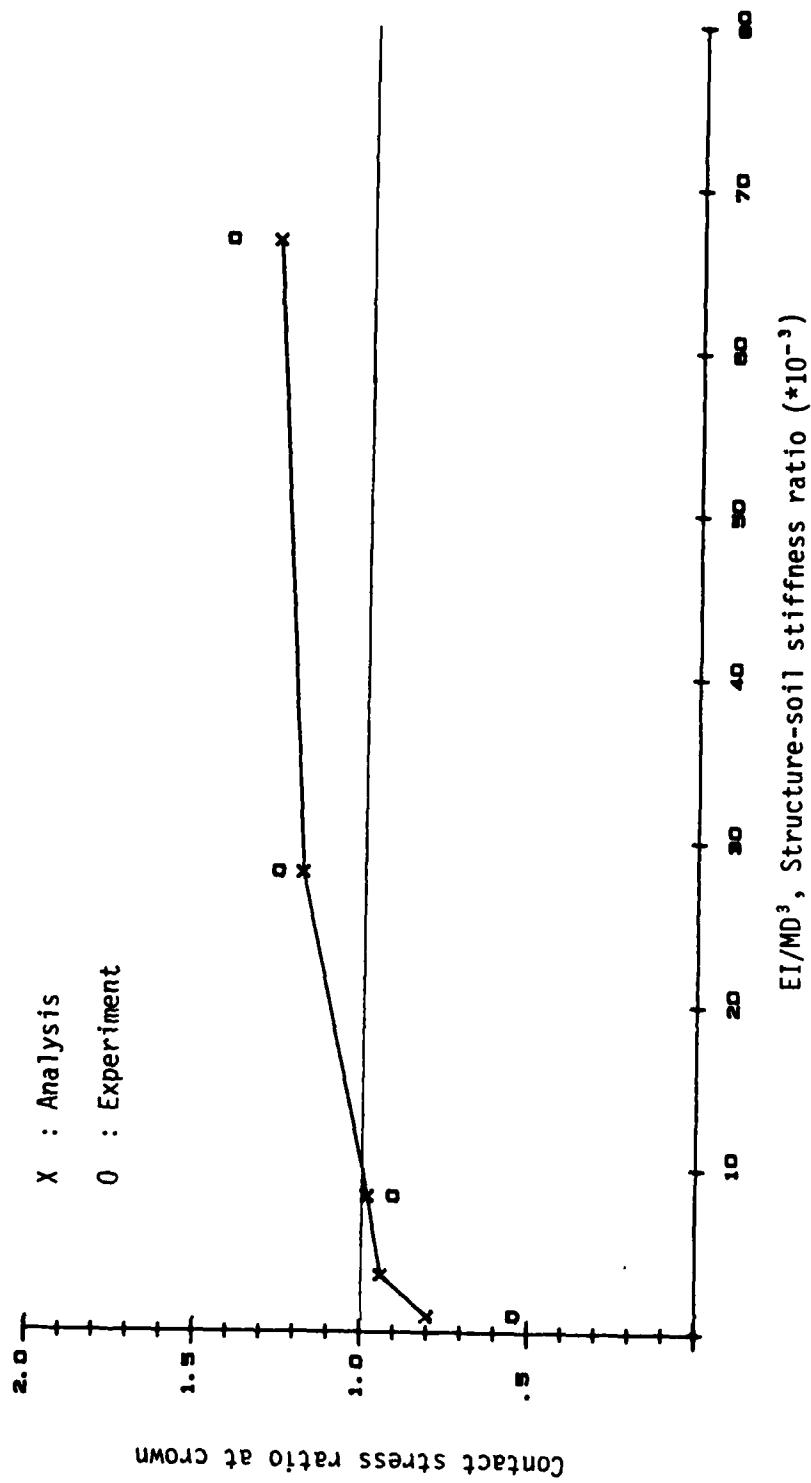


Figure 28. Contact stress ratio at crown vs. structure-soil stiffness ratio for surface overpressure of 90-100 psi

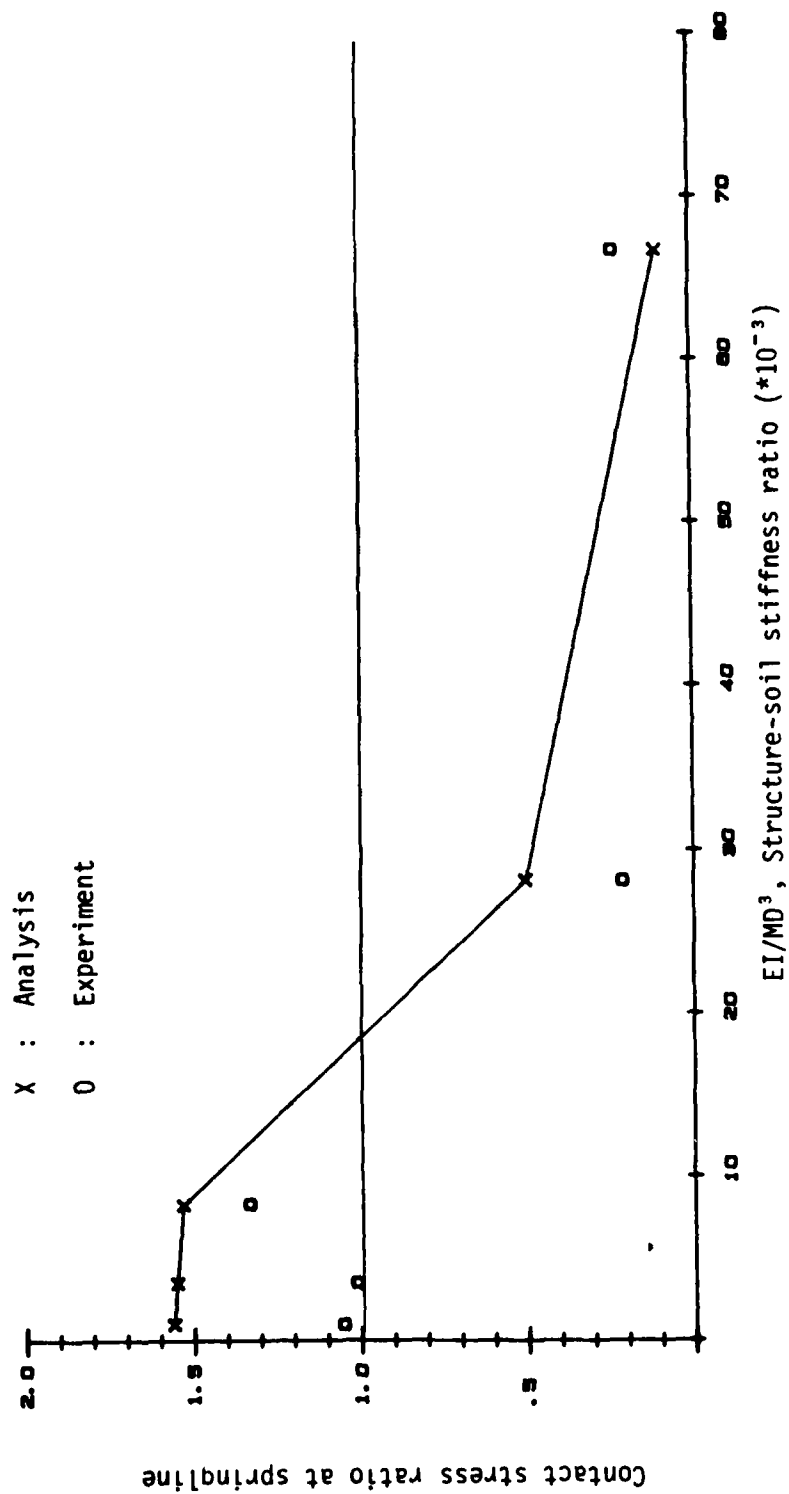


Figure 29. Contact stress ratio at springline vs. structure-soil stiffness ratio for surface overpressure of 90-100 psi

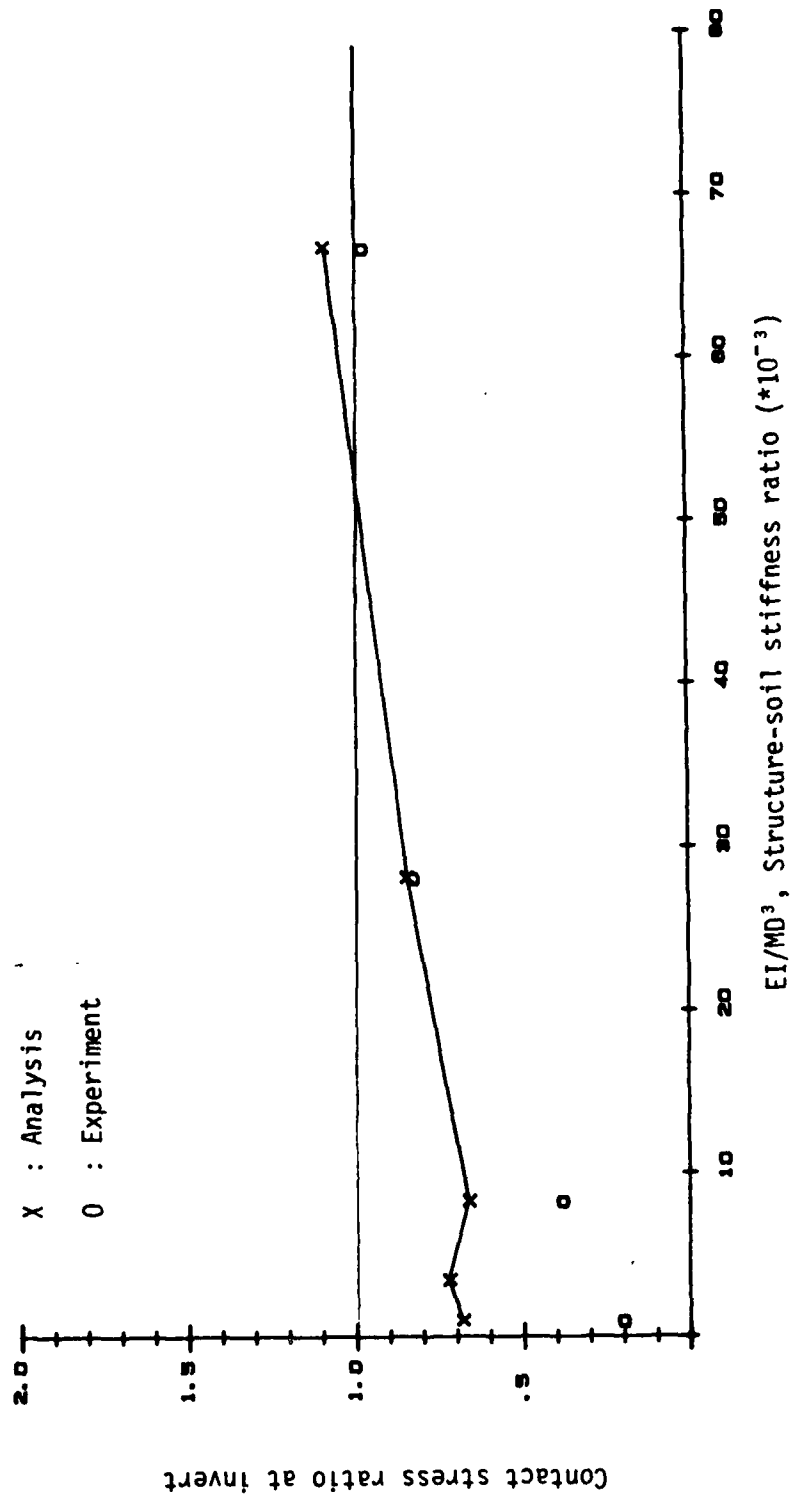


Figure 30. Contact stress ratio at invert vs. Structure-soil stiffness ratio for surface overpressure of 90-100 psi

assured. The user must determine by trial and error the range of conditions for which a stable, and hence meaningful, solution can be obtained from the code.

DATE  
L MED  
8